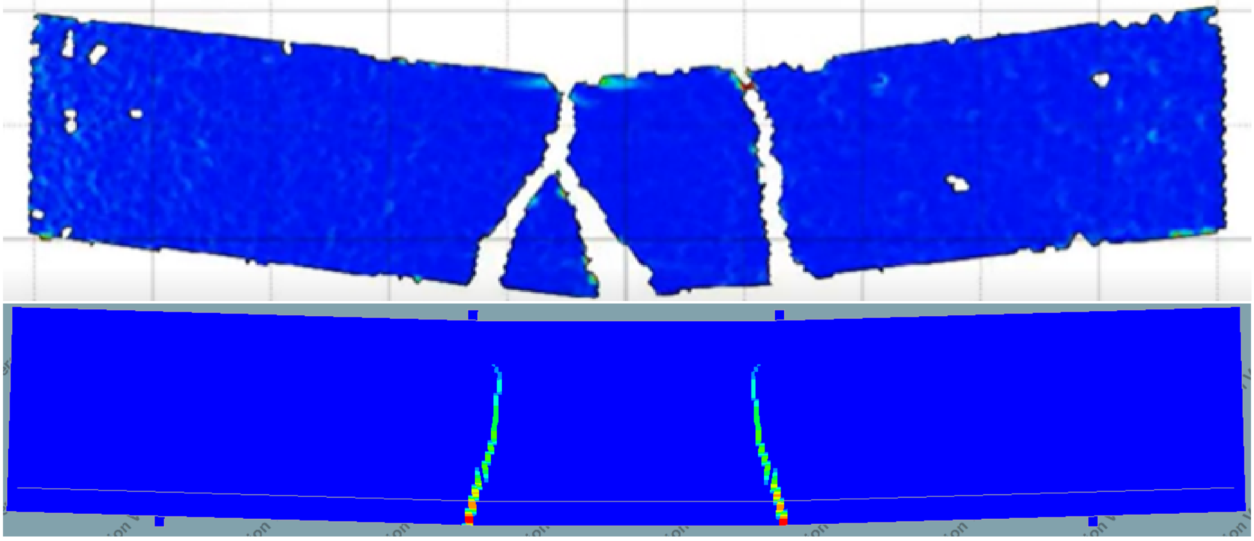

Analysis of carbon reinforced lightweight concrete structures and possible applications

Master's thesis in Master Program Structural Engineering and Building Technology

RASMUS LEVIN

LENNART NYLUND

Department of Architecture and Civil Engineering
CHALMERS UNIVERSITY OF TECHNOLOGY
Master's thesis ACEX30
Gothenburg, Sweden 2023

Master's thesis ACEX30

Analysis of carbon reinforced lightweight concrete structures and possible applications

RASMUS LEVIN
LENNART NYLUND

Department of Architecture and Civil Engineering
Division of Structural Engineering
Concrete Structures Group
Chalmers University of Technology
Gothenburg, Sweden 2023

Analysis of carbon reinforced lightweight concrete structures and possible applications
RASMUS LEVIN, LENNART NYLUND

Supervisor: Karin Lundgren, Department of Architecture and Civil Engineering
Examiner: Karin Lundgren, Department of Architecture and Civil Engineering

Department of Architecture and Civil Engineering
Division of Structural Engineering
Concrete Structures Group
Chalmers University of Technology
SE-412 96 Gothenburg
Telephone +46 31 772 1000

Cover: Figures of crack patterns in the experiment and FE-analysis of Beam 3, just before failure.

Department of Architecture and Civil Engineering
Gothenburg, Sweden 2023

Carbon fibre reinforced lightweight concrete
RASMUS LEVIN, LENNART NYLUND
Department of Architecture and Civil Engineering
Chalmers University of Technology

Abstract

Steel-reinforced concrete has made intricate constructions feasible for more than the past hundred years. There are many benefits of using this effective composite although the service life is challenged by reinforcement corrosion. For applications where a low dead weight is necessary, lightweight concrete (LWC) has become an alternative to normalweight concrete (NWC). However, the drawbacks to LWC are that it is vulnerable for reinforcement corrosion and have a low tensile strength compared to NWC. Still, there is a potential way forward to create lightweight structures that are simultaneously resistant to corrosion. To explore this alternative further, new reinforcement materials must be investigated, e.g. carbon fibre reinforcement (CFR). The material has advantages due to the corrosion resistance of the carbon reinforcement, but carbon bundles and cords have problems with low bond strength between the carbon reinforcement and the concrete, as well as interfilament slip in the reinforcement. Currently, there is a large gap in research regarding the pros and cons of CFR and understanding of how CFR can be optimized using different methods. This study is an attempt to close that gap and provide some answers.

To gain knowledge of the behaviour of the reinforcement and the interaction with the concrete, pull-out and four-point bending tests with carbon fibre reinforcement in straight bundles and braided cords have been carried out prior to this thesis. The data from the pull-out experiments were analysed and the data that were deemed characteristic were used as input to a bond stress versus slip model applied in the FE-program DIANA. This bond-slip model was used in FE-analyses of the four-point bending tests, and the results were compared to the experimental results. Finally, the bond-slip model was used in analyses of stocky columns, where the carbon reinforcement was used to provide lateral confinement.

The analyses of the tests proved that the CFR had a low bond strength to the LWC and that only a few percent of the strength and stiffness of the materials was utilised. The analyses gave a good resemblance to the experimental results, thus they gave a good estimation of the behaviour of the composite. The knowledge gained was further used to discuss suitable applications, e.g. floating pontoons, sewage culverts and edge beams used for bridges. This study attempted to fill the gaps in research regarding CFR in LWC. In the future, more research within this field will be pivotal to further broaden the scope of potential applications and evaluate both advantages and disadvantages.

Keywords: Carbon fibre reinforcement, CFR, Lightweight concrete, LWC, Bond slip, Interfilament slip, Pull-out test, Four-point bending test, FE-model

Kolfiberarmerad lättbetong
RASMUS LEVIN, LENNART NYLUND
Institutionen för arkitektur och samhällsbyggnadsteknik
Chalmers tekniska högskola

Sammanfattning

Stålarmad betong har gjort det möjligt att skapa invecklade konstruktioner i över hundra år. Det finns många fördelar med att använda denna effektiva komposit, även om livslängden utmanas av korrosion av armeringen. För tillämpningar där låg egenvikt är nödvändig har lättbetong blivit ett alternativ till normal betong. Nackdelarna med lättbetong är emellertid dess sårbarhet mot armeringskorrosion och låg draghållfasthet jämfört med normal betong. Trots detta finns det en potentiell väg framåt för att skapa lättviktiga strukturer som samtidigt är motståndskraftiga mot korrosion. För att undersöka denna alternativa möjlighet ytterligare måste nya armeringsmaterial undersökas, till exempel kolfiberarmering. Materialet har fördelar på grund av kolfiberarmeringens korrosionsbeständighet, men kolfiberbuntar och rep har problem med låg vidhäftningshållfasthet mellan kolfiberarmeringen och betongen, samt glidning mellan filamenten i armeringen.

För närvarande finns det en stor kunskapslucka när det gäller för- och nackdelar med kolfiberarmering och förståelsen för hur kolfiberarmering kan optimeras med olika metoder. Denna studie är ett försök att fylla den luckan och ge några svar.

För att få kunskap om beteendet hos armeringen och interaktionen med betongen har dragprov och fyrpunktsböjningstest med kolfiberarmering i raka buntar och rep genomförts före denna avhandling. Data från dragproverna analyserades och den karakteristiska datan användes som indata till en modell för vidhäftningsspänning som applicerades i FE-programmet DIANA. Denna vidhäftnings-modell användes i FE-analyser av fyrpunktsböjningstesterna, och resultaten jämfördes med de experimentella resultaten. Slutligen användes vidhäftnings-modellen i en analys av kraftiga pelare, där kolfiberarmeringen användes för lateral inneslutning.

Analysen av testerna visade att kolfiberarmeringen hade låg vidhäftningshållfasthet till lättbetongen och att endast några få procent av draghållfastheten och styvheten var nyttjade. Analyserna gav en god överensstämmelse med de experimentella resultaten, därigenom gav de en bra uppskattning av kompositens beteende. Den erhållna kunskapen användes sedan för att diskutera lämpliga tillämpningar, såsom flytande bryggor, avloppsledningar och kantbalkar för broar. Denna studie försökte fylla kunskapsluckorna när det gäller kolfiberarmering i lättbetong. I framtiden kommer mer forskning inom detta område att vara avgörande för att ytterligare bredda möjligheterna med potentiella tillämpningar och utvärdera både fördelar och nackdelar.

Nyckelord: Kolfiberarmering, Lättbetong, Armerings glidning, Glidning mellan fibrer, Dragprov, Fyrpunktsböjnings test, FE-modell

Acknowledgements

We want to thank Luping Tang and Sebastian Almfeldt for the data provided and all answers to our questions about the experimants. We also want to thank Langzi Chang for the fast response when we where stuck in DIANA. We want to thank Mia Engman for helping us with reviewing the text. We also want to thank our families and friends for all the support we have gotten during the progress of this master thesis. Finally, we want to give an extra large thank you to our examiner and supervisor Karin Lundgren for all the help and interesting discussions during this master thesis.

Rasmus Levin and Lennart Nylund, Gothenburg, June 2023

Contents

Abstract vi

Sammanfattning viii

Acknowledgements ix

List of Figures xiii

List of Tables xvii

1 Introduction 1
1.1 Background 1
1.2 Aim and objectives 2
1.3 Method 2

2 Lightweight concrete and carbon fibre reinforcement 3
2.1 History and use of today: concrete, lightweight concrete and reinforced concrete 3
2.2 Lightweight concrete 4
2.3 Carbon fibre reinforcement 5
2.4 Bond and interfilament slip 6

3 Experiments 9
3.1 Pull-out tests 10
3.2 Four-point bending tests 13

4 Finite element analysis 17
4.1 Pull-out tests 17
4.1.1 Model 17
4.1.2 Convergence study 20
4.2 Four-point bending 21
4.2.1 Model 21
4.2.2 Convergence study 23

5 Results and Discussion 25
5.1 Pull-out tests 25
5.2 Four-point bending tests 28
5.2.1 Beam 1 30

5.2.2 Beam 2 . . . 31
5.2.3 Beam 3 . . . 32
5.2.4 Beam 4 . . . 33
5.2.5 Beam 5 . . . 34
5.2.6 Beam 6 . . . 35
5.2.7 Beam 7 . . . 36
5.2.8 Beam 8 . . . 37
5.3 General observations and comparisons . . . 38

6 Applications 39
6.1 Stocky columns . . . 39
6.2 Floating pontoons . . . 42
6.3 Culvert . . . 42
6.4 Edge beams . . . 42
6.5 Discussion . . . 42

7 Conclusions 43

References 45

A Appendix 1 I
A.1 Pull-out test . . . I
A.1.1 Inter-filament slip . . . II
A.2 Four-point bending test . . . III
A.2.1 Material data . . . III
A.2.2 Moment in four-point bending test . . . IV
A.2.3 First crack . . . VII
A.2.4 Maximum stresses . . . VII

List of Figures

2.1 Illustration of bond- and interfilament slip. 7

3.1 Images from Tang (2022). The Left figure displays the straight bundle reinforcement. The right figure displays the braided cord reinforcement. 10
3.2 Cross-sections for the pull-out tests. The left figure is the general cross-sections of the specimens. The right figure is the cross-section at the notch of the specimens. 11
3.3 Pull out test specimens. SB-75, SB-150, and SB-300 had straight bundle carbon reinforcement and BC-75, BC-50, and BC-65 had braided carbon cord reinforcement. 11
3.4 Measurements of the beams that have been tested in four-point bending. 13
3.5 Cross-sections of the different beams, showing type of concrete and reinforcement. Properties of concrete types C1-C4 are given in Table 3.4. 14
3.6 Illustration of four-point bending test. 15

4.1 Picture of the FE-model used in the pull-out analysis, showing boundary conditions and the applied load. 18
4.2 The final bond-slip curve defining the different variables used in the Bond-slip material model. 20
4.3 Effect of varying element size. Graphs showing the load-displacement curves, from tests and analyses of pull-out test BC-75. 21
4.4 Picture of the FE-model used in the four-point bending analysis, showing boundary conditions and the applied load. 22
4.5 Graphs showing the differences of the load-displacement curves, between various amount of load steps used in the four-point bending test. 24

5.1 Diagrams of load-displacement relation for the pull-out tests. 25
5.2 Diagrams of load-displacement relation for the pull-out tests. Note the different scales in the diagrams. 26
5.3 Graphs showing the results from each test of the different analyzes, using the chosen element size of 0.004[m]. Note that the dotted line represents tensile failure in the reinforcement. 27

5.4 Pictures showing the stress distribution in the reinforcement at the maximum load. Also tables showing the stress levels with the capacity as the maximum value. The first picture is BC-75, the picture in the middle is BC-50 and the last picture is BC-65. 28

5.5 The cross-section for Beam 1 is presented together with the results of the experiment and the FE-analysis. The crack patterns at different stages are marked in the diagram. A - First crack in the experiment. B - Right before failure in the experiment. C - First crack in the FE-analysis. D - Final load step in the FE-analysis. Note the different scale in the diagram compared to the other beams. 30

5.6 The cross-section for Beam 2 is presented together with the results of the experiment and the FE-analysis. The crack patterns at different stages are marked in the diagram. A - First crack in the experiment. B - Right before failure in the experiment. C - First crack in the FE-analysis. D - Final load step in the FE-analysis. Note the different scale in the diagram compared to the other beams. 31

5.7 The cross-section for Beam 3 is presented together with the results of the experiment and the FE-analysis. The crack patterns at different stages are marked in the diagram. A - First crack in the experiment. B - Right before failure in the experiment. C - First crack in the FE-analysis. D - Final load step in the FE-analysis. 32

5.8 The cross-section for Beam 4 is presented together with the results of the experiment. The crack patterns at different stages are marked in the diagram. A - First crack in the experiment. B - Right before the large pull-out of the reinforcement occur. 33

5.9 The cross-section for Beam 5 is presented together with the results of the experiment and the FE-analysis. The crack patterns at different stages are marked in the diagram. A - First crack in the experiment. B - Right before failure in the experiment. C - First crack in the FE-analysis. D - Final load step in the FE-analysis. 34

5.10 The cross-section for Beam 6 is presented together with the results of the experiment and the FE-analysis. The crack patterns at different stages are marked in the diagram. A - First crack in the experiment (Beam 6). B - Right before failure in the experiment (Beam 6). C - First crack in the experiment (Beam 6´). D - Right before failure in the experiment (Beam 6´). E - First crack in the FE-analysis. F - Final load step in the FE-analysis. 35

5.11 The cross-section for Beam 7 is presented together with the results of the experiment and the FE-analysis. The crack patterns at different stages are marked in the diagram. A - First crack in the experiment. B - Right before failure in the experiment. C - First crack in the FE-analysis. D - Final load step in the FE-analysis. 36

5.12 The cross-section for Beam 8 is presented together with the results of the experiment. The crack patterns at different stages are marked in the diagram. A - First crack in the experiment. B - Just prior to the significant deformations in the experiment. Note the different scale in the diagram compared to the other beams. 37

6.1 Model of a stocky column, with distributed load on top and boundary conditions on the bottom. 40
6.2 Left diagram show the convergence study. The right diagram are showing the differences in load-carrying capacity between the various columns. Note the different scales. 41
6.3 Pictures of the reinforcement stresses and tables over the highest stress in the reinforcement. In the left picture the BC-reinforcement is shown and in the right the steel reinforcement is shown. 41

A.1 Showing the ratios between utilised and not utilised area in the reinforcement cross-section. III
A.2 Setup of the bending test with global measurements, loads and reaction forces. IV
A.3 Section at 0m $<$ x $\leq$ 0.3m. V
A.4 Section at 0.3m $<$ x $\leq \frac{L}{2}$. VI
A.5 Moment diagram in the beam between the supports. Maximum moment is 0.15P. VII
A.6 Model over force-equilibrium in the cross-section in the beam after the first crack have appeared. VIII

List of Tables

3.1 Material data of the SB-reinforcement, from the producer. 9
3.2 Material data of the BC-reinforcement, from the producer. 9
3.3 Embedded length and tensile strength for each of the test specimens. 10
3.4 Material data for the concrete in the four-point bending test. 14
3.5 Material properties of the concrete used in four-point bending test. E_{cm}, $f_{ctk,0,05}$, f_{ctm} and $f_{ctk,0,95}$ is presented for C1. E_{lcm}, $f_{lctk,0,05}$, f_{lctm} and $f_{lctk,0,95}$ is presented for C2, C3 and C4. 15

4.1 Material data of the concrete used in the pull-out tests. 18
4.2 Reinforcement properties and Bond-slip relation between the concrete and the surface area of the reinforcement. 19
4.3 Reinforcement cross-section area, that was active in the analyses. The contact perimeter between the concrete and the reinforcement. 20
4.4 The differences of material data for the concrete in the bending tests, compared to the concrete in the pull-out tests, in Table 4.1. 22
4.5 Steel reinforcement properties in the reference beam, Beam 1. 22
4.6 Showing the reinforcement cross-section area that were active in the analyses of the four-point bending tests. Also the contact area between the concrete and the reinforcement. 23
4.7 Number and length of the load steps in the convergence study, applied in the four-point bending analysis. 23

5.1 Maximum load, tensile stress, failure mode, utilisation ratio of the tensile strength and maximum average bond stress for each of the specimens. For detailed calculations see Appendix A.1. 26
5.2 Load, displacement, moment and stress at the first crack for each of the beams. 29
5.3 Maximum load after first crack, displacement, Failure mode, moment and stresses obtained from four-point bending tests. Utilisation ratios for the reinforcement and the concrete. For the failure modes, FTF means flexural tensile failure, FF means flexural failure, POF means pull-out failure and SF means shear failure. 29

6.1 Table with maximum load and capacity increase for each column, and maximum reinforcement stress and force for the columns with steel and BC-reinforcement 41

A.1 Input data from the test set-ups (embedded length, l, and tensile strength, f_t) and the maximum force, F_{max}, obtained in the tests. . . I
A.2 Calculated values of maximum stresses, the utilisation ratio of the reinforcement strength and the maximum mean shear stresses between the concrete and the reinforcement. II
A.3 Material properties for each of the concrete types. Values obtained by interpolation of values in Table 3.1 in EC2. Note that this not the final modulus of elasticity and tensile strengths of the types that are LWC. III
A.4 Final material propeties for the LWC types. IV
A.5 Showing the force in which the first crack appear in the concrete, as well as the cracking moment and the cracking stress for the first crack. VII
A.6 Young's modulus for the reinforcment and the concrete in the top of the beam, together with α and the number of reinforcement bars, n. . VIII
A.7 Reinforcement area, A_s, and neutral plane, x, for each of the beams tested in four-point bending VIII
A.8 Results from the hand calculations for the beams tested in four-point bending. IX

1

Introduction

1.1 Background

Steel-reinforced concrete has enabled complex structures over a hundred years ago which have stood the test of time until this very day (Moussard et al., 2018). The main imperatives to develop reinforced concrete were economic and fire safety reasons. Even though steel-reinforced concrete is an effective composite with several benefits such as previously mentioned, it does have drawbacks. The concrete cracking exposes the reinforcement and leads to reinforcement corrosion. The porosity of the concrete increases the risk for corrosion even without direct exposure of the reinforcement due to carbonation.

For applications where a low dead weight is beneficial, lightweight concrete (LWC) has been proposed as an alternative. As it is more porous, the problem with steel corrosion in LWC structures is even larger than for ordinary concrete (Haque et al., 2004). For concrete with lightweight aggregate, a larger concrete cover is needed to protect the steel reinforcement (European committee for standardization, 2004). Further, LWC has a lower tensile strength than normal weight concrete (NWC).

To enable light and slender structures without corrosion problems, alternative reinforcement materials can be used. One alternative is to use carbon fibre reinforcement (CFR), which in combination with LWC are in focus in this thesis. Reinforcing with carbon fibres can be done in different ways, either by the use of bars like glass fibre reinforced plastic (GFRP) rebars or as textile reinforcement. The carbon textile reinforcement consists of many filaments in forms of bars or grid-like meshes. The filaments in the bars are either bundled or braided together. This thesis will investigate the difference of these two types of bars, in larger bundles or rope-like structures. The filaments in the carbon fibre reinforcement can be split up in two groups, inner and outer filaments. The outer filaments are directly bonded to the concrete while the inner filaments are bonded to other filaments by friction and have no bond directly to the concrete (Hegger & Voss, 2008). When the friction bond between the inner filaments is insufficient, slip between the filaments occur, called interfilament slip. Further, slip occurs also between the outer filaments and the concrete, which together with interfilament slip can result in an apparent reduction in strength and stiffness of the yarn (Sciegaj et al., 2022).

1.2 Aim and objectives

The aim was to develop and verify a modelling strategy capable of describing the structural behaviour of carbon fibre reinforced LWC, and to use that to investigate possible suitable applications. To reach this aim, the following objectives were outlined;

- Analyse available test data to understand the behaviour of carbon reinforcement and LWC.
- Investigate the difference between braided cord reinforcement and straight bundle reinforcement.
- Develop FE-models that describe the structural behaviour of carbon fibre reinforced LWC.
- Use the modelling method to find suitable applications for carbon fibre reinforced LWC.

1.3 Method

The project started with a literature study to gain knowledge about carbon fibre reinforced LWC. This knowledge was used to analyse results from four-point bending and pull-out tests previously done. The results from the experiments were used to develop FE-models in Diana. The knowledge from the test results and the modelling method was then used to investigate possible applications. The investigation was done by looking at advantages and disadvantages of the material and which applications this is most suitable for.

2

Lightweight concrete and carbon fibre reinforcement

This chapter discusses literature that underpin the experiments that are discussed in this thesis. The origins of concrete, LWC, and reinforced concrete are discussed followed by an outline of the properties of LWC. Studies covering the properties of CFR are explained, including interfilament slip.

2.1 History and use of today: concrete, lightweight concrete and reinforced concrete

Concrete is a material that has been used for a century and a half (Firty, 2012). Other types of concrete were also experimented with and used as early as antiquity. This was when the benefits of using lightweight aggregates were discovered which were the ancestral idea to what today is LWC. Romans used aggregate with natural deposits in concrete for the construction of harbour piers along the west coast of Italy.

The strength and durability of concrete was elevated by the introduction of reinforcement. This was realised in the second half of the 19th century (Firty, 2012). Consequently, steel-reinforced concrete started to become more broadly used in the middle of the twentieth century for multi-story building and long span bridges (Bogas & Real, 2019). In 1886, E L Ransome built the first reinforced concrete bridge in North America which is still in service today (Moussard et al., 2018). This speaks of how revolutionising reinforced concrete became then and has remained even to this day.

Aside from benefits concerning strength and durability, other dimensions have become important in the contemporary discussion regarding reinforced concrete. The awareness of the environmental impact from CO_2 emissions has become vast a global concern as a new discourse commenced by the First Session of the IPCC published by IPCC (1988). The issue became an acknowledged topic of interest due to the financial rationale by Stern (2007) and Gore (2007) whom succeeded in reaching a wider audience. These works set a clear starting point for what later became a matter of debate and transition. As of this reason it has become important to dissect the contributions to climate change from different sectors. According to IEA and GlobalABC (2019), buildings and construction accounted for 39% of CO_2 emissions globally, and of that proportion building materials, including concrete, accounted for 11% of emissions in 2018. The report concluded that there is a need for more sustainable materials to reduce environmental impact of materials in the buildings and construction value chain. Lifecycle approaches are further emphasised in the report and it has become part of the design to elucidate the need for high permanence of structures. It is worth noting that the extent of CO_2 emissions is usually higher for lightweight aggregate concrete (LWAC) than that of normal weight cement due to larger proportions of total cementititous materials content. The reason for the larger porportion is to ensure workability, pumpability and avoid weakening the strength development (Kanavaris et al., 2020). However, the paper by Junaid et al. (2022) puts the scope of LWC in to a broader purpose by unfolding the idea that waste byproducts from industries and agriculture could be utilised as an aggregate, admixture and cementing agent in LWC. From a life cycle and consumption perspective, this application could prove to be part of both environmental protection and sustainable development. In addition, the shortening of the lifetime of structures is often due to the degradation of the steel bars. The use of reinforcement which is less prone to corrosion can prolong the lifetime of structures. In this way, new materials can form composites that are more effective both environmentally and structurally.

2.2 Lightweight concrete

LWC is a group of concrete-like materials with the common goal to have both good bearing capacity and insulating ability (Burström & Nilvér, 2018). The primary difference between LWC and NWC is that LWC is much lighter. The density ranges up to 2200 kg/m^3, while normal concrete which varies between 2400-2500 kg/m^3 (Kanavaris et al., 2020). Even though LWC has been used for a long time, less is known about the durability performance of LWC compared to NWC (Bogas et al., 2019). The most common materials in Sweden from this group are autoclaved aerated concrete and LWAC (Burström & Nilvér, 2018). LWAC is similar to NWC but uses LWC combined with an aggregate with lower density and is more porous (Burström & Nilvér, 2018).

LWAC makes structures lighter which for certain applications enables smaller cross-sections of structural parts due to less dead weight of the structure (Bremner, 2008). Another advantage with LWAC is that it has much better insulation properties than regular concrete due to higher porosity, resulting in a lower thermal conductivity. For this reason, LWC is an appropriate building material for the climate shell in housing (Kanavaris et al., 2020).

Although there are many benefits to using LWAC over NWC there are also disadvantages. LWAC is more brittle and exhibit more uncontrolled cracking compared to NWC, in particular when subjected to compression (Zivkovic et al., 2018). However, according to Byard and Schindler (2010) this issue could be mitigated to a certain extent by using pre-wetted light weight aggregate to reduce early-phase cracking. Zivkovic et al. (2018) elaborates on the matter and suggest that the addition of fibres can handle this issue.

To better understand the durability of reinforced concrete it is important to recognise the effects of carbonation, which is one of the most common reasons for degradation. The process of carbonation is a physochemical reaction between carbon dioxide and the alkalinity of concrete prompted by calcium hydroxide and calcium silicate hydrate (Lo et al., 2008). According to Bogas and Real (2019), carbonation resistance is found to be lower for LWAC than that of NWC and the reason is the higher porosity of the LWAC. The carbon dioxide diffusion rate is dependent on the characteristics of the porous structure of the concrete. For reinforced concrete with aggregates the high porosity will benefit the carbon dioxide diffusion, ultimately leading to lower carbon resistance and unfavour the durability of LWAC compared to NWC.

2.3 Carbon fibre reinforcement

Two alternative reinforcement methods, as a substitution for ordinary steel reinforcement, are fibre-reinforced plastic (FRP) rebars and textile reinforcement (Friese et al., 2022). A benefit of using textile reinforcement, and also FRP rebars, compared to steel is that textile reinforcement is corrosion resistant which enables a smaller concrete cover. This leads to decreased use of concrete which lowers the overall CO_2 emissions (Friese et al., 2022). The emissions from producing the same weight of carbon fibre textile reinforcement are 8 times higher than from the production of steel reinforcement (Stoiber et al., 2021). However, a study by Scope et al. (2020) has shown that the weight of the reinforcement needed to secure the same properties as for a wall application. These properties were 22 times higher than needed for the textile reinforcement. This results in a significant reduction of CO_2 emissions.

FRP rebars are rebars made of plastic that are reinforced most commonly with glass- (GFRP), basalt- (BFRP), aramid- (AFRP) or carbon fibre (CFRP) (Mirdarsoltany et al., 2022). To create a better bond between the FRP rebars and the concrete, the rebar-surface can be conducted in different ways, e.g. by milling, sanding/roughening, or wrapping it with FRP roving (Friese et al., 2022).

Textile reinforcement is made of hundreds or thousands of filaments bundled or braided together. The fibre materials that are normally used as textile reinforcement are glass- (GF), basalt- (BF), and carbon fibre (CF) (Friese et al., 2022).

Successful applications using textile reinforcement in concrete have been conducted in areas of construction where the flexibility of reinforcement is needed to form free-form shape structures (Friese et al., 2022). Another successful application for carbon mats is for the purpose of strengthening existing structures to enable old structures to carry more load or to prolong the lifetime of structures. In this application, the usage of carbon mats glued or bonded by cementitious mortar to the outside of the concrete to strengthen structures in places where high stresses are located. This limits further cracking and increases the load-carrying capacity. This method is also used to strengthen concrete slabs after holes have been cut out from the slab

(Carolin, 2003).

Thicker carbon bundles and braided cords are researched, but not yet used in practical applications. Abd et al. (2023) showed that carbon bundles used as shear stirrups performed better than steel in both ductility properties as well as maximum load carrying capacity for beams loaded in bending.

Carbon fibre is an anisotropic material which means that the material has different features in different directions. These different features are affecting the performance of the carbon reinforcement, depending on the arrangement of the fibres. Carbon fibres are strong in the axial direction, along the fibres, but weak in the transverse direction (Duan et al., 2019). In cases when the fibres are braided together, the shear force is induced in the reinforcement even though the force is applied axially, due to the braiding of the fibres creating an angle between the force and the line of fibres.

2.4 Bond and interfilament slip

The bond between carbon filaments and concrete is weaker compared to regular steel reinforcement and concrete, which increases the risk of bond slip (Bilek et al., 2017). This creates a need for a longer anchor length for the carbon reinforcement to use its full potential. Another problem that can occur in carbon fibre bundles or cords is that filaments in the inner part of the reinforcement can slip relative to each other, if they are not properly impregnated (Mechtcherine et al., 2020). This is called interfilament slip and occurs when the shear force between the outer layer and the inner layer of the reinforcement is higher than the frictional force between the filaments, see Figure 2.1 for illustration. When interfilament slip occurs the inner filaments are deactivated, and the outer filaments connected to the matrix will carry a heavier load due to this effect (Zhu et al., 2021). While the load progresses, the tensile force in the outer filaments increases until the tensile capacity is reached, thus filaments in the outer layer rupture. Ultimately this leads to the weakening of the reinforcement and the composite as a whole. The objective is to create a good bond between the concrete and the outer fibres and activate the inner core of the reinforcement. To reduce both interfilament- and bond slip in textile-reinforced concrete, a common solution is to impregnate the reinforcement with either polymer- or mineral-impregnation (Friese et al., 2022), (Schneider et al., 2019). The effect of the impregnation is however reduced if the bundle or cord is not homogeneously or fully impregnated (Friese et al., 2022).

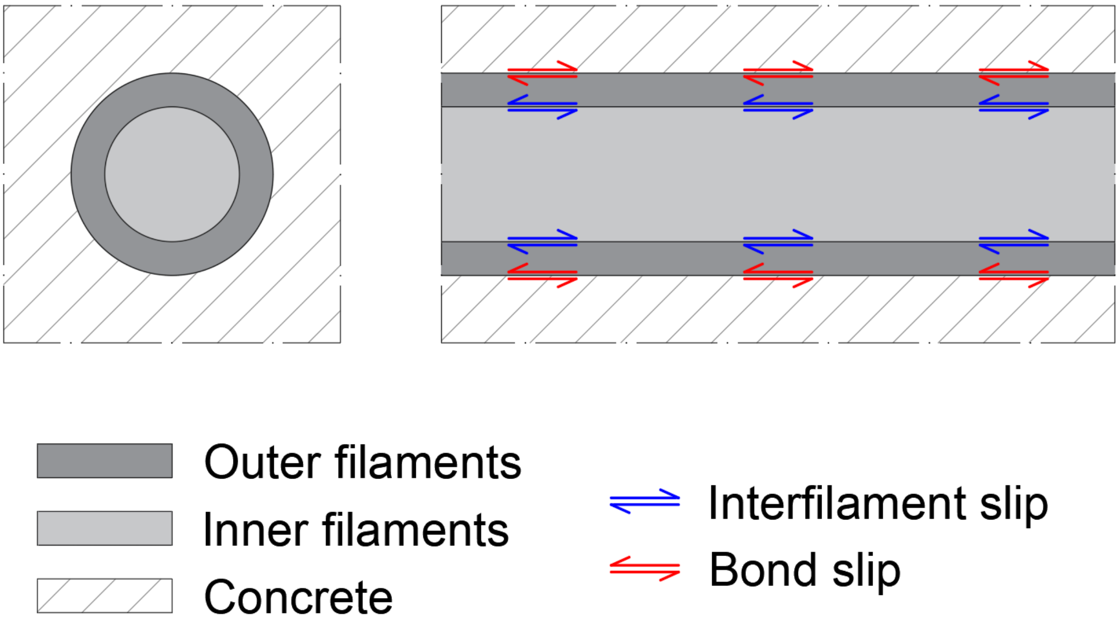

Figure 2.1: Illustration of bond- and interfilament slip.

3

Experiments

Pull-out and four-point bending tests have been performed at the Structures Laboratory at Chalmers University of Technology, before this thesis was done. The information and data from the experiments have been gathered from Tang (2022) and direct conversation with Luping Tang and Sebastian Almfeldt. In this chapter, the test procedures are introduced.

Two types of CFR have been used in the pull-out and the four-point bending tests, one type with straight bundles (SB) and one type with braided cords (BC), see Figure 3.1. Material data of the reinforcement types are presented in Table 3.1 and Table 3.2. Both types of reinforcement have been purchased from Carbix AB and the SB-reinforcement is called Roving Tenax STS40 24K 1600 tex. Both reinforcement types have also been impregnated with an electrochemical method. For the BC-reinforcement, the lower value of f_t, from the producer, was later used in the analysis to not overestimate the theoretical strength of the carbon.

Table 3.1: Material data of the SB-reinforcement, from the producer.

Reinforcement type	Rovin Tenax STS40 24K 1600 tex
Density [g/cm^3]	1.77
Tensile strength, f_t [MPa]	4000
Young's modulus (Tension) [GPa]	240
Elongation at break [%]	1.7
Filament count [-]	24000
Filament diameter [μm]	7
Cord diameter [mm]	8

Table 3.2: Material data of the BC-reinforcement, from the producer.

Reinforcement type	Carbon braided cord
Density [g/cm^3]	1.76-1.78
Tensile strength, f_t [MPa]	3530-4210
Young's modulus (Tension) [GPa]	230
Cord diameter [mm]	7.5
Weight [g/m]	39.4

Figure 3.1: Images from Tang (2022). The Left figure displays the straight bundle reinforcement. The right figure displays the braided cord reinforcement.

3.1 Pull-out tests

Six pull-out tests had been carried out, three with SB-reinforcement and three with BC-reinforcement. The SB-reinforcement had a diameter of 8[mm] and the ones with BC-reinforcement had a diameter of 7.5[mm]. The embedded CFR had been casted in the centre of each specimen, which had a size of 80x80x800[mm], see Figure 3.2 and 3.3. The concrete surrounding the CFR had been reinforced with four steel rebars, each with a diameter of 8[mm], see Figure 3.2. After about two months of curing of the concrete, the pull-out tests were performed. The concrete at the time of testing had a compressive strength of 19.2[MPa] and a density of 1450[kg/m^3]. A notch was made by cutting at a 45-degree angle around the CFR at a depth resulting in cutting of the steel rebars, leaving only 30x30[mm] of concrete, see Figure 3.2. The notch was cut at different lengths of the specimens to give the carbon reinforcement different embedded lengths. The specimens with SB-reinforcement had been cut at 75, 150 and 300[mm] respectively and the specimens with BC-reinforcement were cut at 50, 65 and 75[mm] respectively, see Figure 3.3. Displacement-controlled tests were performed to each of the specimens until either tensile failure or pull-out failure of the CFR occurred. The embedded length and the tensile strength of the reinforcement for each of the specimens is presented in Table 3.3.

Table 3.3: Embedded length and tensile strength for each of the test specimens.

Specimen	SB-75	SB-150	SB-300	BC-75	BC-50	BC-65
Embedded length [mm]	75	150	300	75	50	65
f_t [MPa]	4000	4000	4000	3530-4210	3530-4210	3530-4210

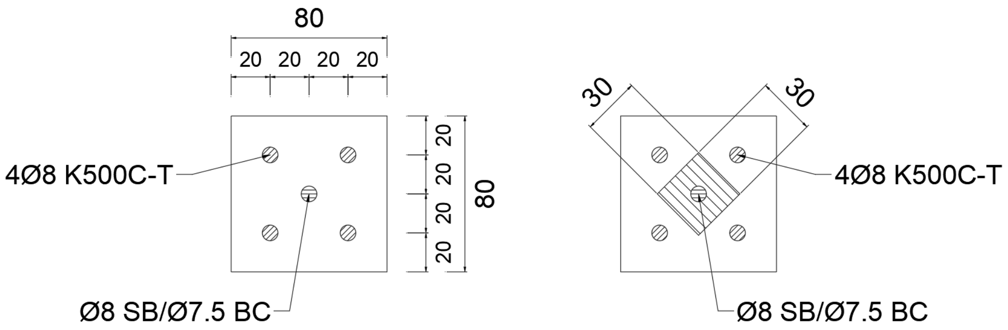

Figure 3.2: Cross-sections for the pull-out tests. The left figure is the general cross-sections of the specimens. The right figure is the cross-section at the notch of the specimens.

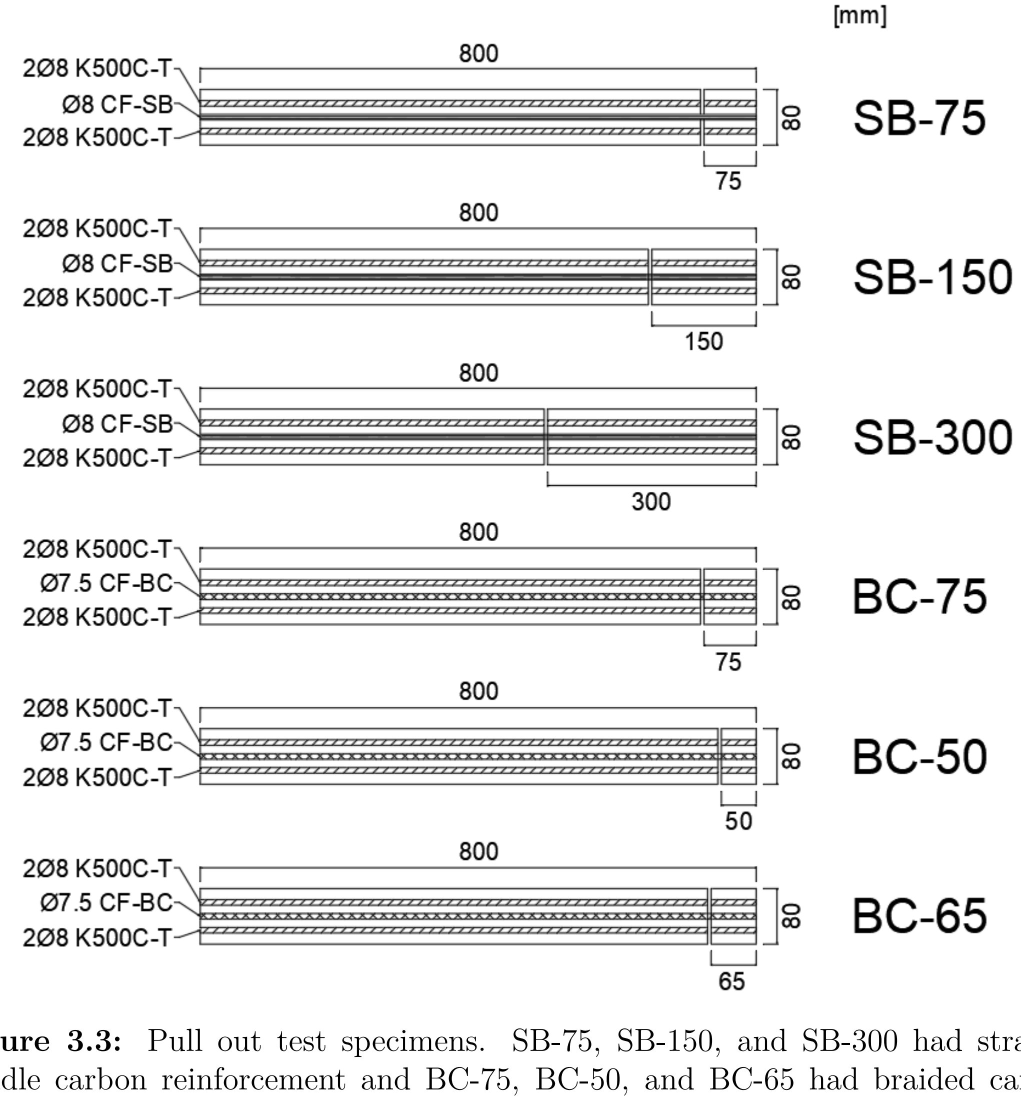

Figure 3.3: Pull out test specimens. SB-75, SB-150, and SB-300 had straight bundle carbon reinforcement and BC-75, BC-50, and BC-65 had braided carbon cord reinforcement.

The experiments resulted in reinforcement pull-out in all samples except in specimen BC-75 where tensile failure occurred. The tests started out by testing both types of reinforcement with an embedded length of 75[mm]. For this embedded length, the SB-reinforcement resulted in pull-out failure. Due to this failure mode, the SB-reinforcement was tested for a longer embedded length of 150[mm], trying to distinguish at which embedded length tensile failure first occur. Even in the second test the SB-reinforcement reinforcement was pulled out. The last test with SB-reinforcement was performed with an embedded length of 300[mm], yet also this test resulted in pull-out failure. In this test, pull-out of the reinforcement was stopped at a length of about 150[mm] due to the maximum travel of the machine was reached.

For the BC-reinforcement, the first test, with an embedded length of 75[mm] resulted in tensile failure. Also in this case, the goal was to distinguish at which embedded length the reinforcement alternates between different failure modes. Therefore, the second test was performed with a shorter embedded length of 50[mm]; at this length the specimen was subjected to pull-out failure. The third test was performed with an embedded length of 65[mm], i.e. in between the two lengths with different failure modes. For this test, pull-out failure occurred once again.

From the pull-out tests, data had been obtained by logging the relation between tensile force and elongation of the specimens. In addition, digital image correlation (DIC) had been used, enabling detailed measurements of the displacement field including the crack opening over the notch.

3.2 Four-point bending tests

Nine concrete beams with various amount and configurations for the embedded reinforcement had been casted with various layers of concrete. Beam 1 had been casted with K500C-T steel reinforcement embedded in C40/50 concrete. This beam was used as a reference of ductility, crack pattern and maximum stresses for a standard reinforced concrete beam subjected to bending. C40/50 concrete had been used in the compressive zone in all beams except Beams 3 and 4. The measurements and cross-sections of the different configurations can be seen in Figure 3.4 and Figure 3.5. DIC had been used to capture the crack-pattern of the beams while performing the bending tests.

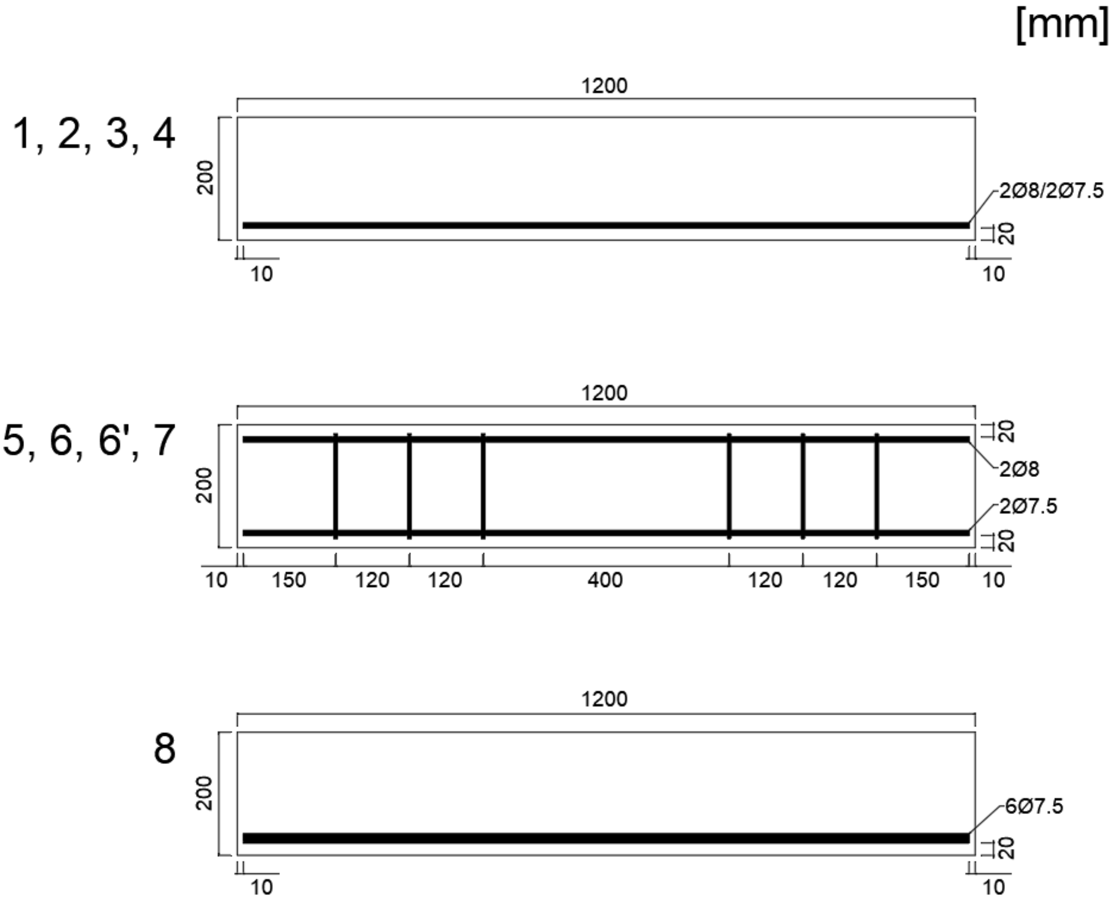

Figure 3.4: Measurements of the beams that have been tested in four-point bending.

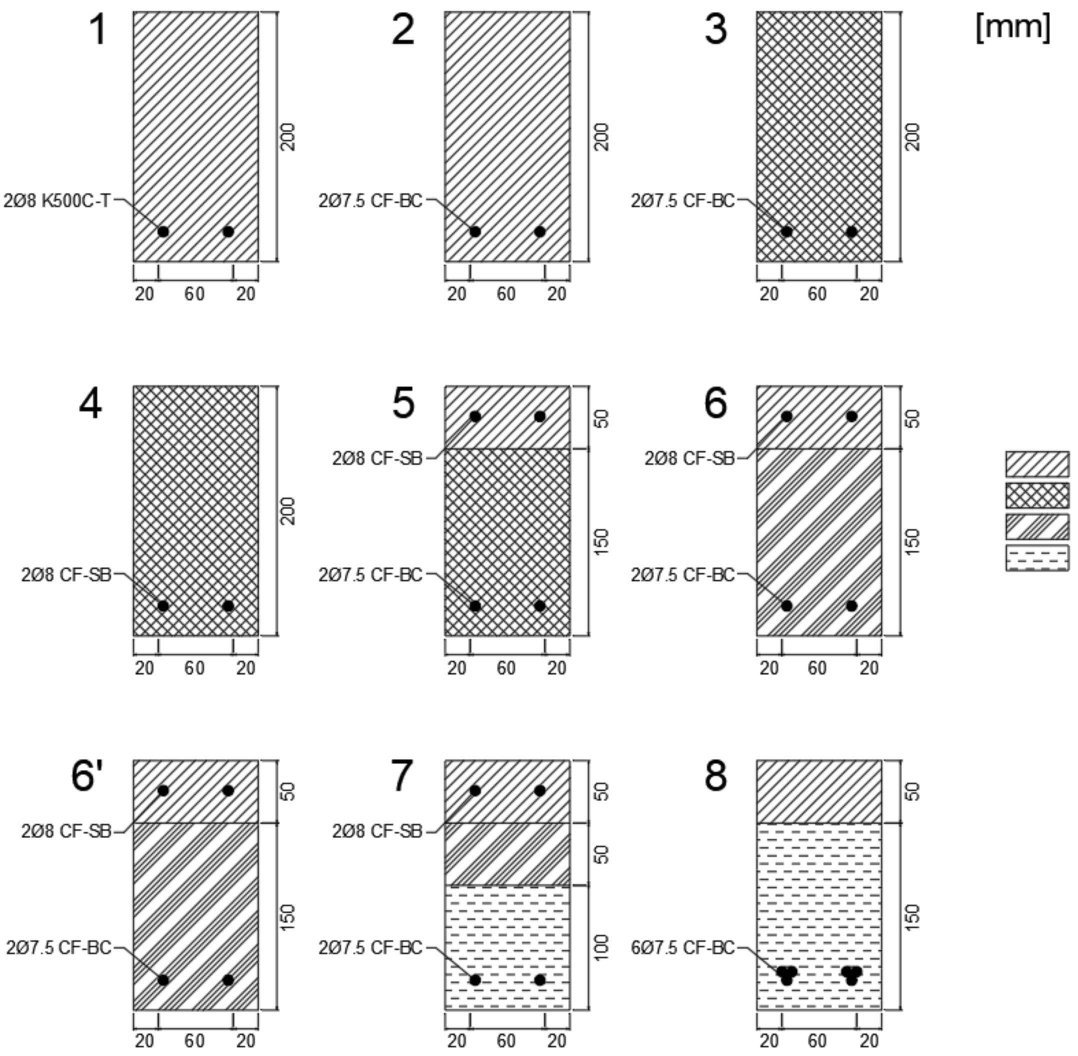

Figure 3.5: Cross-sections of the different beams, showing type of concrete and reinforcement. Properties of concrete types C1-C4 are given in Table 3.4.

All the beams had been loaded via four-point bending tests. The tests had been set up on two supports with a spacing of 900[mm] in between and the load had been applied with 300[mm] of spacing between the two loading points, see Figure 3.6. The concrete material data from material tests in Chalmers Structures Laboratory is presented in Table 3.4.

Table 3.4: Material data for the concrete in the four-point bending test.

Concrete type	C1	C2	C3	C4
Apparent density [kg/m^3]	2460	1450	1520	1260
Compressive strength [MPa]	49.8	21.6	19.2	17.5

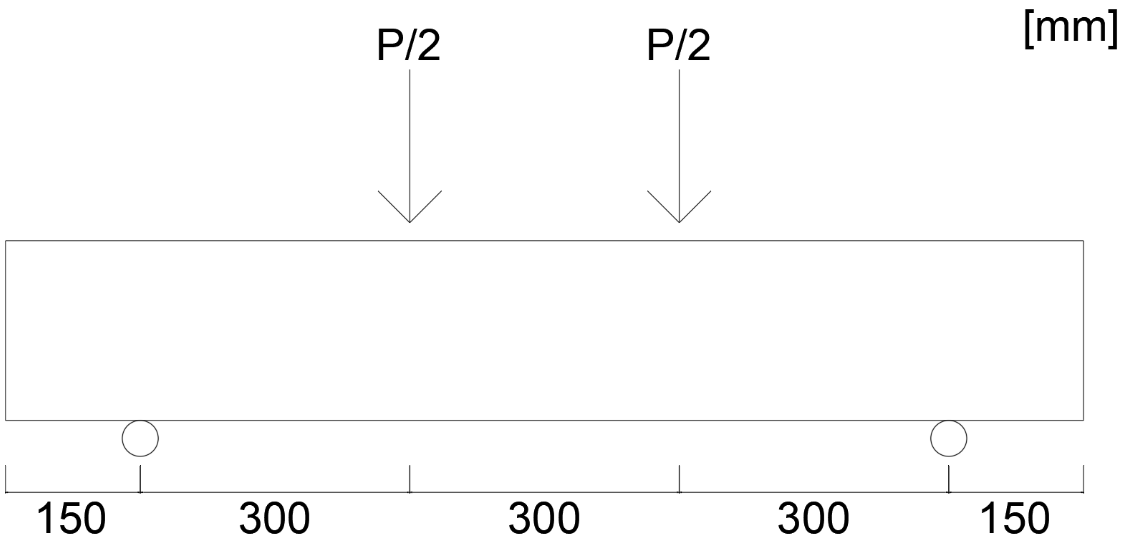

Figure 3.6: Illustration of four-point bending test.

The material properties of the different concrete types, in Table 3.5, were derived from interpolation between values from Table 3.1 in (European committee for standardization, 2004). For the different light-weight concrete types, the derived values were multiplied by factors, from Table 11.3.1 in (European committee for standardization, 2004), based on the density of each concrete type. Detailed calculations can be seen in Appendix A.2.1.

Table 3.5: Material properties of the concrete used in four-point bending test. E_{cm}, $f_{ctk,0,05}$, f_{ctm} and $f_{ctk,0,95}$ is presented for C1. E_{lcm}, $f_{lctk,0,05}$, f_{lctm} and $f_{lctk,0,95}$ is presented for C2, C3 and C4.

Concrete type	C1	C2	C3	C4
E_{cm} and E_{lcm} [GPa]	35.36	12.08	12.70	8.45
$f_{ctk,0,05}$ and $f_{lctk,0,05}$ [MPa]	2.57	0.94	0.86	0.73
f_{ctm} and f_{lctm} [MPa]	3.61	1.37	1.25	1.05
$f_{ctk,0,95}$ and $f_{lctk,0,95}$ [MPa]	4.71	1.75	1.55	1.25

4

Finite element analysis

This chapter describes the computer-modeling of the pull-out and four-point bending experiments. The models was analysed in the FEM-program Diana. When creating the models, focus was set to only model the specimens with braided chord reinforcement. The reason for this choice was that there was no available test data for rupture of the SB-reinforcement, as all the pull-out tests on that reinforcement type resulted in pull-out failure. While for the specimens with BC-reinforcement, pull-out test of the specimen BC-75 was loaded to tensile failure of the cord. The pull-out specimens were modeled to get a bond-slip behaviour between the BC-reinforcement and the concrete similar to the experiments previously done. The bond-slip properties obtained from the pull-out models was later used as input in the four-point bending models. The LWC used in the pull-out experiments differs from the concrete in the four-point bending experiments. This was taken into account in the strength parameters of the different materials, but the bond-slip properties were assumed to be the same in all FE-models.

4.1 Pull-out tests

In this subsection, the FE pull-out models are described. Geometry and boundary conditions as well as material parameters are presented in figures and tables. The bond-slip model is described and also shown in a figure. Finally, a convergence study of the analyses is presented.

4.1.1 Model

The models have the same dimensions and reinforcement configurations as the ones in the experiment. The boundary conditions in the FE-model were chosen to mimic the experimental setup of how the experiments were carried out, see Figure 4.1. The left side was prevented from movement in horizontal direction and a support with prescribed deformation, in load steps, was applied on the right side in horizontal direction. The bottom long-side was also fixed in the vertical direction but was free to deform in the horizontal direction. The only side that was totally free to deform was the top long-side, thereby enabling the model to deform according to Poisson‘s effect. The same load step configuration, with a total 298 load steps, was used in every pull-out analysis: 100 short steps with the length of 0.0001 in the beginning and 198 longer steps with the length of 0.005 afterwards. The shorter steps in the beginning were applied to get a detailed analysis of the first crack of the concrete.

A difference between the experiment and the FE-model was that, in the FE-model, the reinforcement was placed 5mm from the edge in both ends to ensure that it wasn't affected by the boundary conditions.

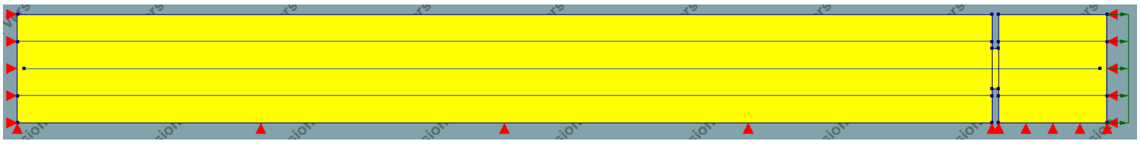

Figure 4.1: Picture of the FE-model used in the pull-out analysis, showing boundary conditions and the applied load.

The material model used for the concrete was Total strain based crack model in the Concrete and masonry class. The material data for the concrete is presented in Table 4.1. The linear material- and strength properties of the concrete was the same in the FE-models as the tested specimens in the experiments. The fracture energy was set to 100[N/m], the value for fracture energy was first taken from table (2.1.4 CEB-FIP Model Code 90), as the value 70[N/m]. When attempting to input the fracture energy into the software, it was observed that the assigned value was insufficient for the analysis to run successfully. Consequently, an iterative process was undertaken, involving the exploration of various fracture energy values in order to achieve a valid analysis. In the process, 100[N/m] gave a satisfying behaviour and was therefore chosen for the concrete in all FE-analyses. To enable cracks to be localised into one element column, the crack bandwidth was set to be one element length. Linear elasticity was used to model the steel reinforcement. The steel reinforcement in the pull-out tests was set to have a linear elastic behaviour with a Young‘s modulus of 200[GPa]. The steel reinforcement was not at focus in the pull-out tests and the loads were never at a level large enough to exceed the linear elastic interval of the steel, therefore the steel reinforcement was simplified in the analysis.

Table 4.1: Material data of the concrete used in the pull-out tests.

Class	Concrete and masonry
Material model	Total strain based crack model
Crack orientation	Rotating
Tensile curve	Hordijk
Compressive curve	Ideal
Young's modulus [GPa]	12.95
Poisson's ratio [-]	0.2
Mass density [kg/m^3]	1450
Tensile strength [MPa]	1.702
Fracture energy [N/m]	100
Crack bandwidth [m]	0.004
Compressive strength [MPa]	19.2

The material model used for the carbon reinforcement was Bond-slip reinforcement in the class Reinforcements with the bond-slip interface failure model set to CEB-

FIB 2010 bond-slip function. The material data for the carbon reinforcement is presented in Table 4.2. Von Mises plasticity was used in the FE-model with a set yield stress limit of 3.53[GPa]. This means that carbon reinforcement in the FE-model was assumed to has an elastic ideal plastic behaviour. This differs from reality where the carbon reinforcement have a brittle behaviour. In Figure 4.3, the plastic part is shown by dotted lines in the load-deflection curves. The plastic part of the load-deflection curve was ignored in the analysis but shown in the graphs for clarification. To be able to describe the bond-slip between the carbon reinforcement and the concrete, a bond-slip curve was defined. The slip parameters have been optimized so that the FE load-deflection curves resembles the curves coming from the experiments. The maximum and ultimate shear stress parameters have been calculated from the experiment data from the BC-50 specimen, using Eq. A.5 in Appendix A.1. The curve point s_0 was set to 0.005 because a fixed value was mandatory in the program. Due to that $\alpha = 1$, the section between zero and s_1 was linear, so in principal the value for s_0 could have been an arbitrary value between zero and s_1. In the model, s_1 and s_2 are in the same point which result in a direct reduction in shear stress capacity after the maximum shear stress is reached. The final bond-slip curve can be seen in Figure 4.2.

Table 4.2: Reinforcement properties and Bond-slip relation between the concrete and the surface area of the reinforcement.

Class Material model	Reinforcements Bond-slip reinforcement
Nonlinear model	Von Mises plasticity
Hardening function	No hardening
Bond-slip interface failure model	CEB-FIB 2010 bond-slip function
Young's modulus [GPa]	230
Poisson's ratio [-]	0.27
Mass density [kg/m^3]	1770
Yield stress [MPa]	3530
Normal stiffness modulus [N/m^3]	1×10^{14}
Shear stiffness modulus [N/m^3]	1×10^{11}
Maximum shear stress, τ_{max} [MPa]	3.109
Ultimate shear stress, τ_f [MPa]	0.892
Relative slip section, s_1 and s_2 [m]	0.008
Relative slip section, s_3 [m]	0.01389

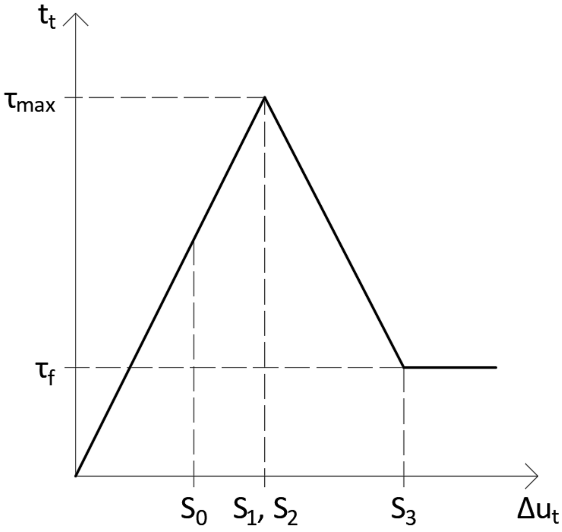

Figure 4.2: The final bond-slip curve defining the different variables used in the Bond-slip material model.

Due to the many filaments in the cords, interfilament slip occur which reduces the utilization of the reinforcement. A utilization ratio was calculated from the results in the experiment analysis. This resulted in a utilisation ratio of 3.34[%] taken from BC-75, see Table A.2 in Appendix A.1. To express this, the cross-section of the carbon reinforcement was reduced to match the strength of reinforcement in the experiment test with BC-75 in every model. In this way, both the strength and the stiffness of the carbon reinforcement cross-section were reduced with the same percentage. Note that the contact perimeter was not reduced, resulting in full contact area between the cord and the concrete in the Diana analysis, see Table 4.3.

Table 4.3: Reinforcement cross-section area, that was active in the analyses. The contact perimeter between the concrete and the reinforcement.

Reinforcement type	Truss bond-slip
Cross-section area of bar [m^2]	1.48×10^{-6}
Contact perimeter [m]	0.0236

4.1.2 Convergence study

The convergence study was carried out by performing BC-75 with three different element sizes of 0.008, 0.004 and 0.002[mm] respectively, see Figure 4.3. The aim of this study was to see where the solution of the analysis between different element sizes were showing similar results, this assured that the analysis were correct. In the convergence study, the solutions converged between element size 0.004 and 0.002[mm]. In order to do faster simulations, the final element size was chosen to the larger of the two. This element size was later used for all pull-out analyses.

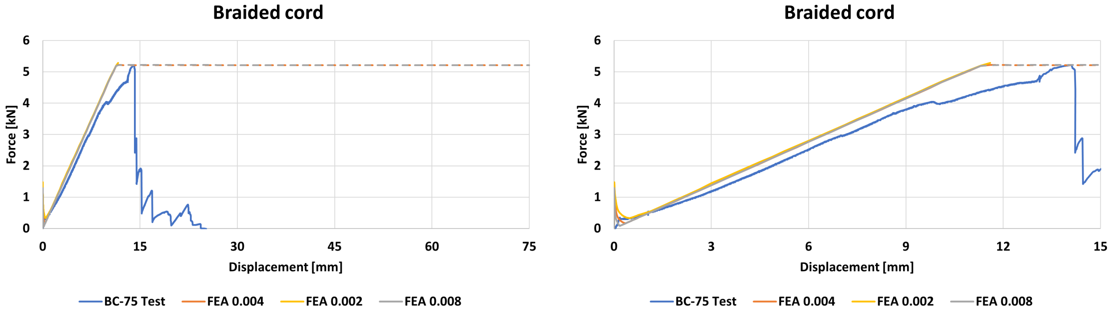

Figure 4.3: Effect of varying element size. Graphs showing the load-displacement curves, from tests and analyses of pull-out test BC-75.

4.2 Four-point bending

In this subsection the FE four-point bending models are described. Geometry and boundary conditions as well as material parameters are presented in pictures and tables, also a convergence study over the analyses is described.

4.2.1 Model

The models, that were analysed in the software DIANA, had the same dimensions and reinforcement configurations as the ones in the experiments. The FE-models was limited to only analyze the specimens with one row of BC-reinforcement, this was due to that the input data from the pull-out analysis only refers to separate BC-reinforcement embedded in the concrete. The boundary conditions in the FE-model was set to describe the way the experiments were carried out. The boundary at the bottom left support was fixed in the horizontal and vertical direction but the rotation was free. The boundary at the bottom right support was also fixed but only in the vertical direction. The loads were applied as a prescribed deformation in negative vertical direction, which was applied in the middle of both the upper supports. The prescribed deformation was applied in loading steps, which simulates the tested specimens in the experiment. To avoid local crushing of the concrete steel plates with cubic shapes of 10x10[mm], have been put in between the concrete and the load on the upper side and between the supports on the bottom side. These steel plates extend through the whole depth of the cross-section of the beams, and distributes the loads on to several elements in the model to avoid local crushing of the concrete. The geometrical model is presented in Figure 4.4.

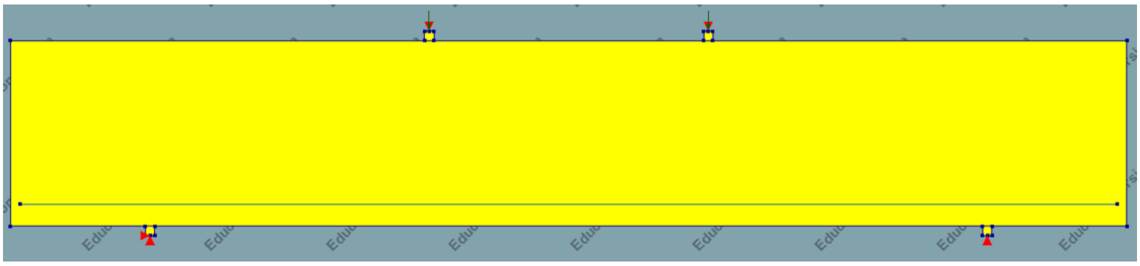

Figure 4.4: Picture of the FE-model used in the four-point bending analysis, showing boundary conditions and the applied load.

There was four different types of concrete in the beams. Each type of concrete was created using the same material model in Diana (Total strain based crack model), but some values in the model differs from each other. The same strength properties were used for each of the concrete types in the experiment and the FE analysis. The values can be seen in Table 4.4. Note that the crack bandwidth was set to one element length, as cracks were assumed to localise into one element column. The steel reinforcement in the reference beam, Beam 1, was modelled with the material model Eurocode 2 EN1992-1-2, and can be seen in Table 4.5.

Table 4.4: The differences of material data for the concrete in the bending tests, compared to the concrete in the pull-out tests, in Table 4.1.

Concrete type	C1	C2	C3	C4
Young's modulus [GPa]	35.36	12.08	12.70	8.45
Mass density [kg/m^3]	2460	1450	1520	1260
Tensile strength [MPa]	3.61	1.37	1.25	1.05
Crack bandwidth [m]	0.0029	0.0029	0.0029	0.0029
Compressive strength [MPa]	49.8	21.6	19.2	17.5

Table 4.5: Steel reinforcement properties in the reference beam, Beam 1.

Class Material model	Reinforcements Eurocode 2 EN1992-1-2
Young's modulus [GPa]	200
Yield stress [MPa]	500
Peak stress [MPa]	575
Strain at peak stress [-]	0.075
Strain at start decay [-]	0.1
Ultimate strain [-]	0.12

The bond behaviour between the reinforcement and the concrete were taken directly from the pull-out analysis. The only difference was that the area of the cord and the contact perimeter have been doubled due to that there were two cords in the bending tests. The bond properties can be seen on Table 4.6.

Table 4.6: Showing the reinforcement cross-section area that were active in the analyses of the four-point bending tests. Also the contact area between the concrete and the reinforcement.

Reinforcement type	Truss bond-slip
Cross-section area of bar [m^2]	2.96 $\times 10^{-6}$
Contact perimeter [m]	0.0471

4.2.2 Convergence study

In analyses of the bending tests, the element size was chosen to be as small as possible in the software using the Education version. Therefore, the convergence study was performed by choosing different loading steps in the analysis. Note that the convergence study of the beams were performed differently from the pull-out tests. The convergence study was carried out by performing the analysis of Beam 3, with three different number of load steps, 265, 530 and 1060 respectively. The analyses were split up into two intervals, the first with shorter load steps, to get a good analysis of the first crack, and the second with longer steps, see Table 4.7. The aim of this study was to see where the solution of the analysis between different load steps showing similar results. This assures that the analysis was correct. The solution converged between load step 530 and 1060. Due to time consuming analysis, the chosen number of load steps were set to 530. The results from the convergence study can be seen in Figure 4.5.

Table 4.7: Number and length of the load steps in the convergence study, applied in the four-point bending analysis.

Number of load steps	First interval	Second interval
265	20 (0.001)	245 (0.004)
530	40 (0.0005)	490 (0.002)
1060	80 (0.00025)	980 (0.001)

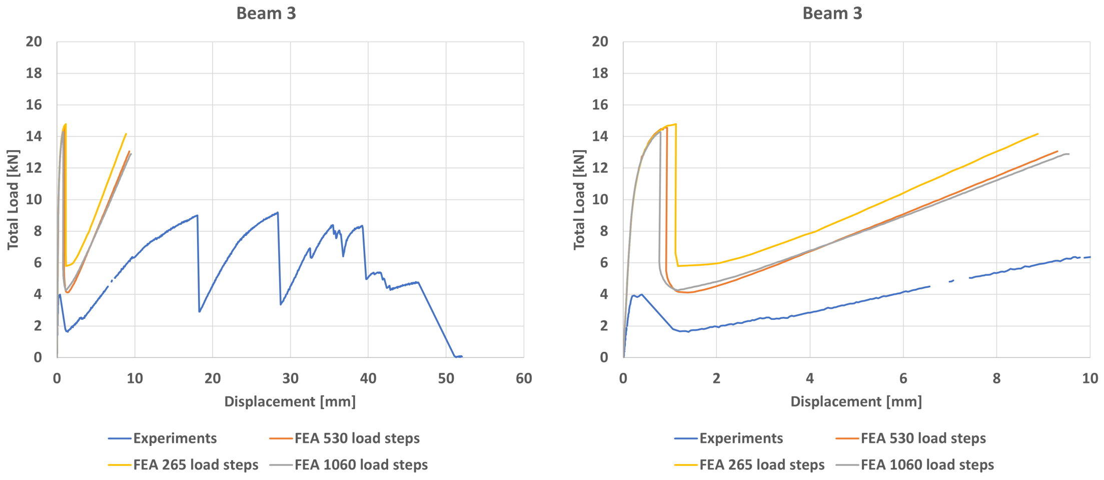

Figure 4.5: Graphs showing the differences of the load-displacement curves, between various amount of load steps used in the four-point bending test.

5

Results and Discussion

This chapter describes the results from the experiments and the FE-analysis and discuss them.

5.1 Pull-out tests

The pull-out test resulted in pull-out failure for all specimens except for BC-75 which demonstrated tensile failure. This was also the result of the FE-analyses of the specimens with the BC-reinforcement. The results will be presented and further discussed in this section.

The load-displacement relation was logged during the pull-out tests. The results can be seen in Figure 5.1 and Figure 5.2. The displacement over the crack opening at the notch was logged and measured using DIC. The maximum force, F_{max}, and failure mode for each specimen can be seen in Table 5.1 together with the calculated maximum tensile stress in the reinforcement, $\sigma_{s,max}$, utilisation ratio U_{σ_s} and maximum average bond stress, τ_b. For detailed calculations see Appendix A.1.

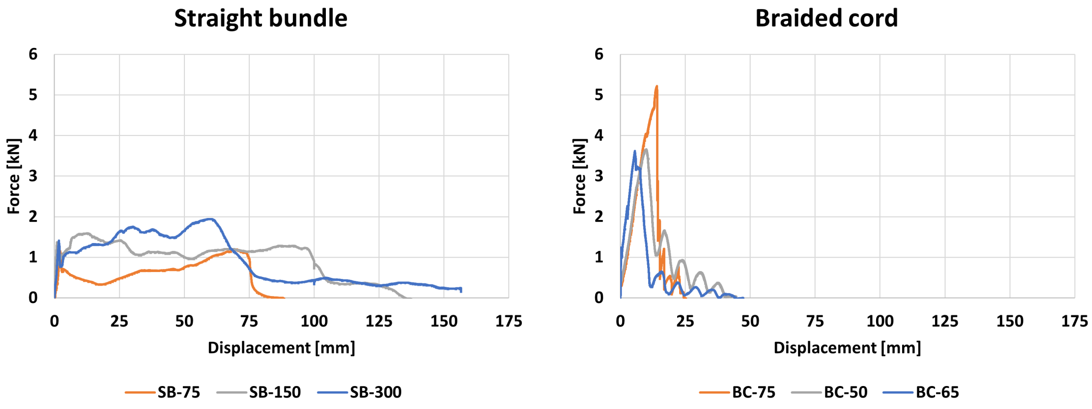

Figure 5.1: Diagrams of load-displacement relation for the pull-out tests.

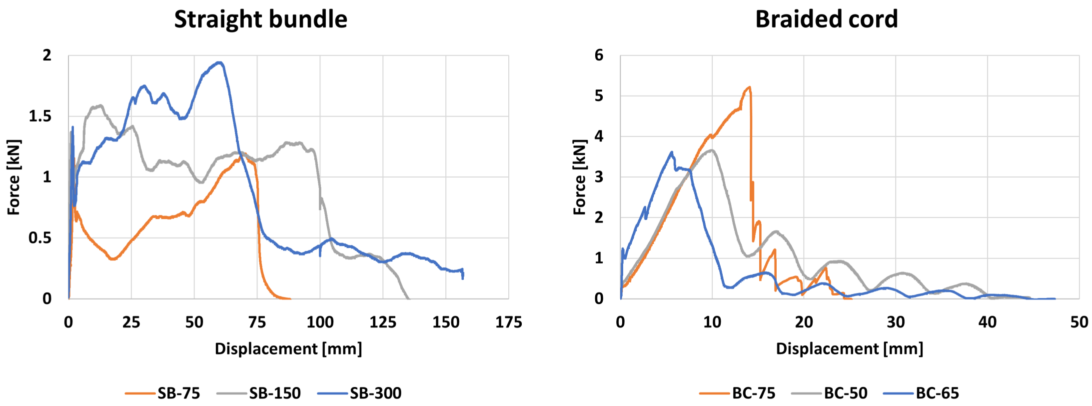

Figure 5.2: Diagrams of load-displacement relation for the pull-out tests. Note the different scales in the diagrams.

All the SB-reinforcement tests resulted in pull-out failure, which makes the actual strength unknown. Thus the specimens with SB-reinforcement are excluded from the FE-analysis. For the tests with BC-reinforcement, tensile failure occured for BC-75 and pull-out failure for BC-50 and BC-65. The maximum tensile stress, $\sigma_{s,max}$, was therefore used from BC-75. The maximum tensile stress, $\sigma_{s,max}$, for BC-75 was 118.08 [MPa] which leads to a utilization ratio, U_{σ_s}, of 3.34 [%], see Table 5.1. The maximum average bond stress, τ_b, resulted in 3.11 [MPa] for BC-50, which was used in the FE-analysis, see Table 5.1.

Table 5.1: Maximum load, tensile stress, failure mode, utilisation ratio of the tensile strength and maximum average bond stress for each of the specimens. For detailed calculations see Appendix A.1.

Specimen	SB-75	SB-150	SB-300	BC-75	BC-50	BC-65
F_{max} [kN]	1.19	1.59	1.94	5.22	3.66	3.62
Failure mode	Pull-out	Pull-out	Pull-out	Tensile	Pull-out	Pull-out
$\sigma_{s,max}$ [MPa]	23.74	31.64	38.66	118.08	82.91	81.95
U_{σ_s} [%]	0.59	0.79	0.97	3.34	2.35	2.32
τ_b [MPa]	0.63	0.42	0.26	2.95	3.11	2.36

The FE-analysis resulted in tensile failure for BC-75 and pull-out failure for BC-50 and BC-65, showing the same results as the experiments. The load-displacement curves from the analysis, in comparison with the experiments, can be seen in Figure 5.3. The FE-analysis and the experiments correlate with almost the same maximum force in both BC-75 and BC-50 as well as with the similar tension build-up. The correlation between the analyses for BC-65 was however not so good, because of the lower bond properties in the experiment compared to the other specimen. A difference in all the FE-analysis compared to the experiments was that the load at which the first crack occur, was lower in the experiments. This could be due to the handling of the tested specimens which could have induced cracks in the notch, thus weakening the concrete. In the FE-analysis, the concrete in the notch was intact, which could explain the differences in tensile strength of the concrete before the first crack occur.

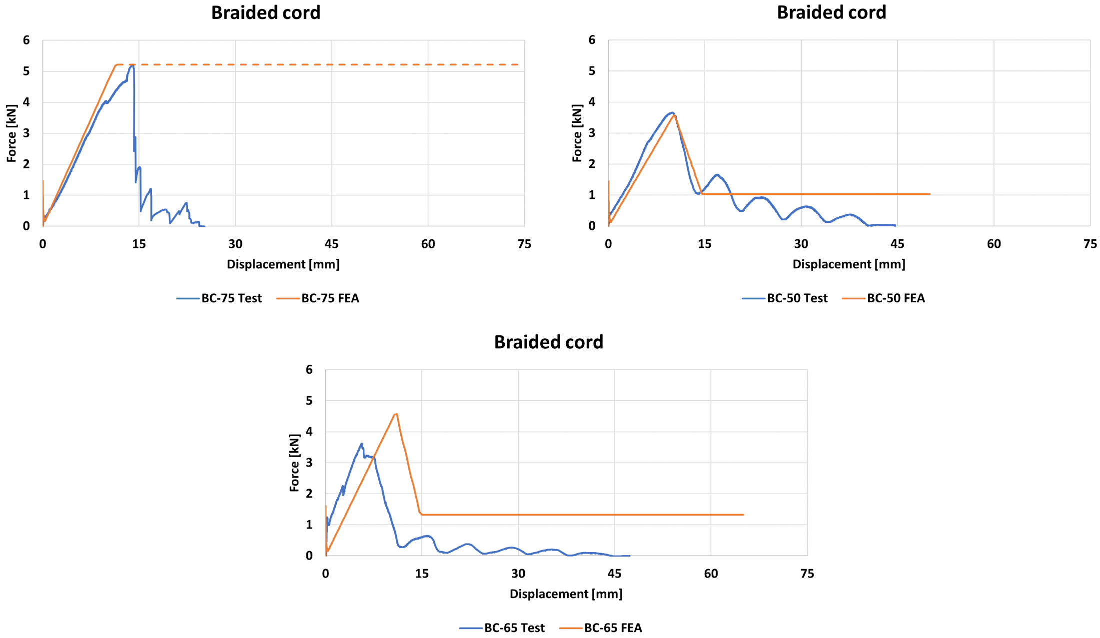

Figure 5.3: Graphs showing the results from each test of the different analyzes, using the chosen element size of 0.004[m]. Note that the dotted line represents tensile failure in the reinforcement.

The resulting stress distribution in the reinforcement at the maximum load are shown in Figure 5.4, which confirms the different failure modes in the FE-analysis. As can be seen, the anchorage length for the carbon reinforcement was considerably larger on the left side which was due to weak bond between the cord and the concrete.

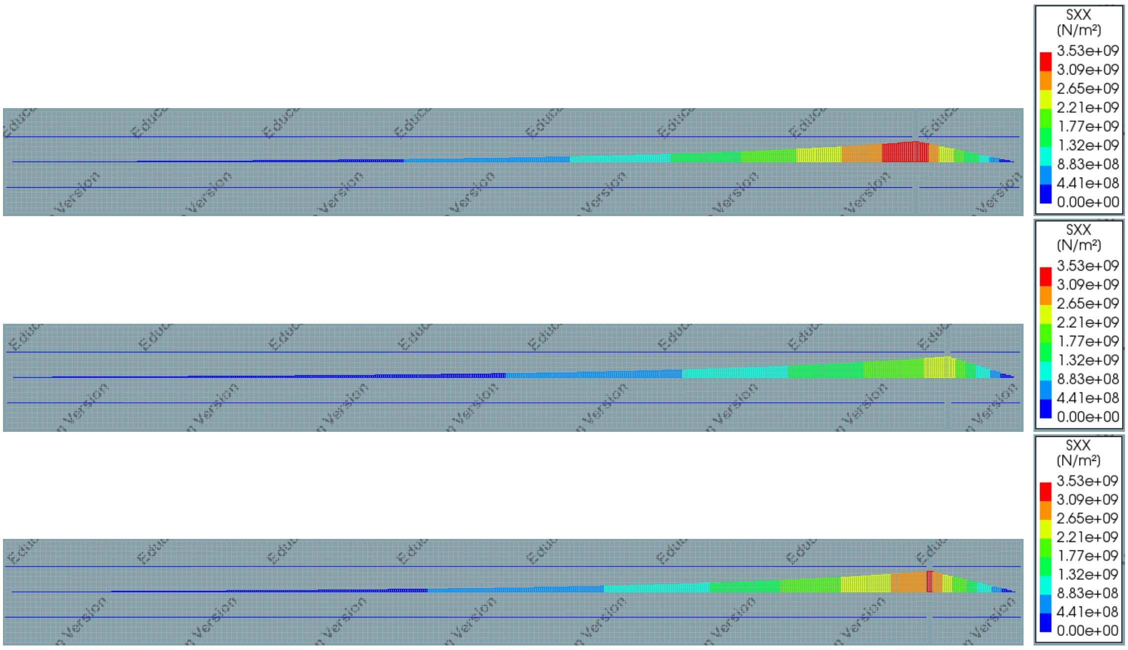

Figure 5.4: Pictures showing the stress distribution in the reinforcement at the maximum load. Also tables showing the stress levels with the capacity as the maximum value. The first picture is BC-75, the picture in the middle is BC-50 and the last picture is BC-65.

5.2 Four-point bending tests

All the beams in the experiments were loaded to failure, and the governing failure mode was flexural tensile failure for all the beams except the reference beam, Beam 1, and the SB reinforced beam, Beam 4. In Beam 1, the reinforcement reached the yield stress limit but was never loaded to total failure of the reinforcement. Tensile failure due to fracture of the reinforcement happened in all of the carbon reinforced beams except Beam 4. In Beam 4, shear cracking with subsequent pull-out of the reinforcement happened. Beam 1 had both the highest maximum load and the smallest deflection, as well as the highest number of cracks. The crack pattern in the carbon-reinforced beams displayed a higher degree of localisation, characterised by fewer cracks with wider crack widths when compared to the reference beam. The SB reinforced beam, Beam 4, was the beam with CFR that could withstand the largest load after the first crack occurred.

The load, F_{cr}, and the displacement, u_{cr}, at the first crack were taken from the experiment data. The cracking moment, M_{cr}, and the stress at the first crack, σ_{cr}, were calculated using the equations in Appendix A.2.3. The results can be seen in Table 5.2.

Table 5.2: Load, displacement, moment and stress at the first crack for each of the beams.

Beam	1	2	3	4	5	6	6´	7	8
F_{cr} [kN]	21.5	16.1	4.0	7.2	14.7	13.0	10.9	12.0	11.4
u_{cr} [mm]	0.4	0.3	0.4	0.5	0.8	0.4	0.3	0.4	0.4
M_{cr} [kNm]	3.2	2.4	0.6	1.1	2.2	2.0	1.6	1.8	1.7
σ_{cr} [MPa]	4.8	3.6	0.9	1.6	3.3	2.9	2.5	2.7	2.6

For the bending tests, the maximum stress in the reinforcement was calculated from force equilibrium in the cross-section. The maximum stress in the reinforcement, $\sigma_{s,max}$, was calculated from the case where the applied vertical force was at maximum after the first crack, F_{max}, resulting in the maximum moment, M_{max}. The utilisation ratios of the reinforcement were obtained by dividing the tensile stress with the tensile strength of the reinforcement, given by the producer. This was also done for the concrete at the outmost compressive part of the beam to determine the compressive strength utilisation of the concrete. The failure modes and the results from the calculations of the tested specimens are shown in Table 5.3. For detailed calculations, see Appendix A.2.4.

Table 5.3: Maximum load after first crack, displacement, Failure mode, moment and stresses obtained from four-point bending tests. Utilisation ratios for the reinforcement and the concrete. For the failure modes, FTF means flexural tensile failure, FF means flexural failure, POF means pull-out failure and SF means shear failure.

Beam	1	2	3	4	5	6	6’	7	8
F_{max} [kN]	62.0	10.5	9.2	18.6	11.5	13.9	12.7	14.7	15.9
u_{max} [mm]	13.3	30.7	52.0	45.3	43.8	60.3	56.0	39.5	93.2
Failure mode	FF	FTF	FTF	POF	FTF	FTF	FTF	FTF	FTF
M_{max} [kNm]	9.3	1.6	1.4	2.8	1.7	2.1	1.9	2.2	2.4
$\sigma_{s,max}$ [MPa]	568.0	96.2	88.9	180.7	105.6	127.9	117.1	135.0	53.2
$\sigma_{c,max}$ [MPa]	29.0	4.6	2.7	5.5	5.1	6.1	5.6	6.5	4.0
$U_{\sigma_{s,max}}$ [%]	113.6	2.7	2.5	4.5	3.0	3.6	3.3	3.8	1.5
$U_{\sigma_{c,max}}$ [%]	58.2	9.3	12.7	25.4	10.2	12.3	11.3	13.0	8.0

In the following subsections, the first crack and the crack pattern at the final load step are presented, along with the load-displacement diagram and cross-section for each of the beams. For all the beams, except Beams 4 and 8, the results from both the experiments and FE-analyses are presented together. It is worth noting that the reinforcement ruptured in every beam with carbon fibre reinforcement in the FE-analysis. This explains the abrupt cutoff of the curves in the diagrams. In Beam 1, which had steel reinforcement, most of the reinforcement yields at the final load step, but no failure occured in the analysis. The maximum compressive stress in the concrete was obtained from the integration points between the loading plates at the top of the beam. The compressive stresses do not reach the compressive strength of the concrete in any of the beams.

5.2.1 Beam 1

Beam 1 was a reference beam with steel reinforcement. In the FE-analysis, the dimensions of the steel plates were doubled in size, compared to in the analyses of the carbon-reiforced beams, to prevent local crushing of the concrete, as this beam was subjected to higher loads. The number of load steps was also reduced to save time while running the analysis. The load-displacement curve is presented in Figure 5.5. As can be seen in the graph, there is a small reduction in the FE curve: this is explained by the first cracking of the concrete. The cracks progress in a scattered pattern for both the FE-analysis and the experimental results, indicating a ductile behavior, see Figure 5.5.

In the FE-analysis, the maximum compressive stress in the concrete was 17.1 [MPa] and the tensile reinforcement reached the yield limit. However, no failure occurred as the ultimate strain of the reinforcement was not reached.

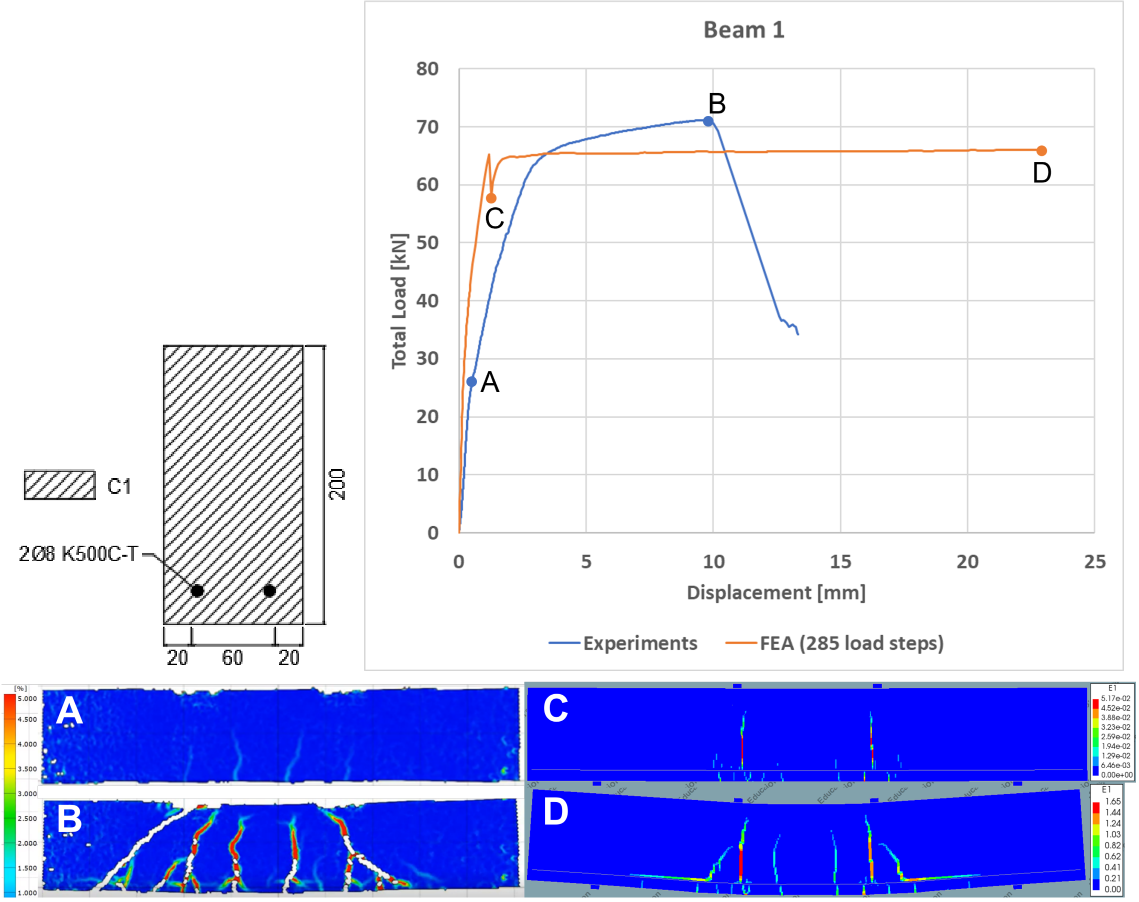

Figure 5.5: The cross-section for Beam 1 is presented together with the results of the experiment and the FE-analysis. The crack patterns at different stages are marked in the diagram. A - First crack in the experiment. B - Right before failure in the experiment. C - First crack in the FE-analysis. D - Final load step in the FE-analysis. Note the different scale in the diagram compared to the other beams.

5.2.2 Beam 2

In the experiment, the crack pattern obtained included only a single crack positioned at the midspan, whereas in the FE-analysis, two cracks were observed closer to the loading points, see Figure 5.6. In the experiment, a plastic hinge was formed within the cracked section, leading to an enlargement of the initial crack, rather than the propagation of tensile stresses into additional cracks. Consequently, the deformation progressed without any significant increase of the load until the reinforcement fractured. The lack of additional cracks indicates a brittle behaviour.

In the FE-analysis, the maximum compressive stress in the concrete was 23.1 [MPa] which is lower than the compressive strength of the concrete. However, the maximum stress in the reinforcement reached its capacity, which led to tensile failure of the reinforcement in Beam 2 at point D in the diagram in Figure 5.6.

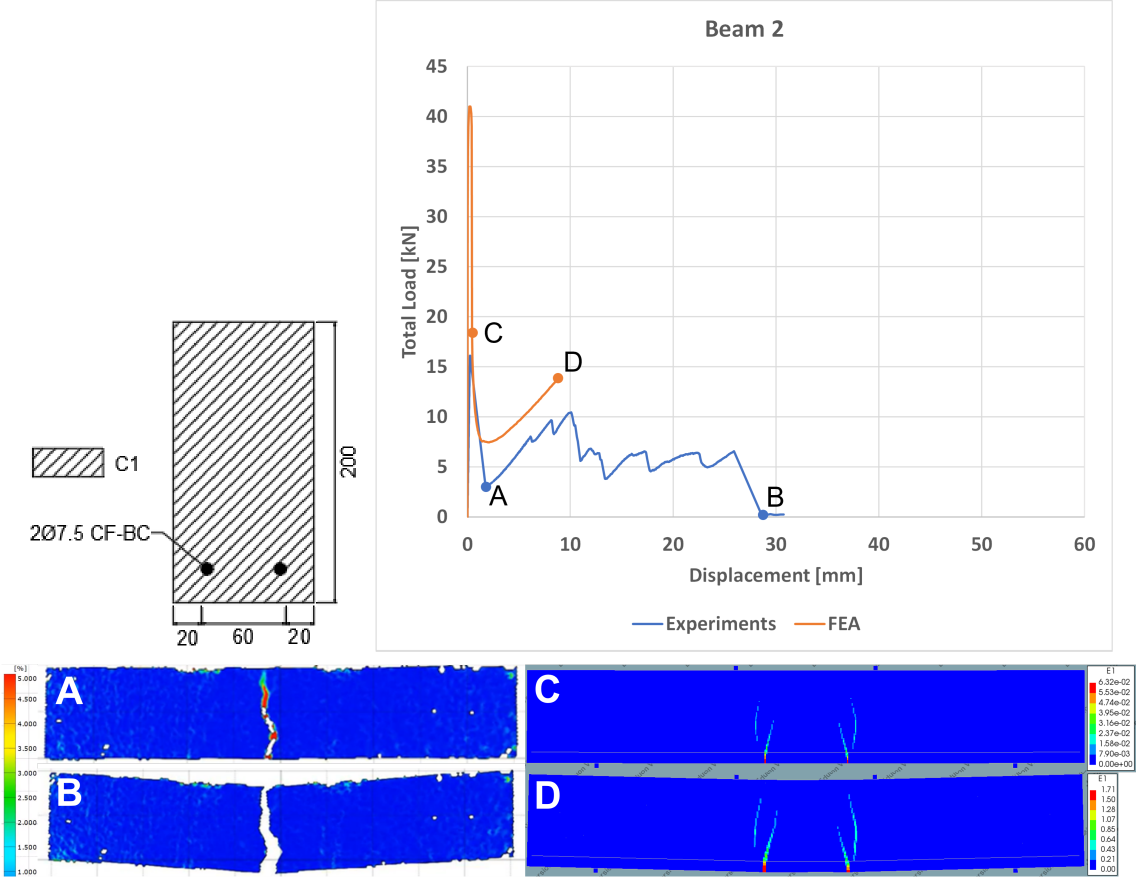

Figure 5.6: The cross-section for Beam 2 is presented together with the results of the experiment and the FE-analysis. The crack patterns at different stages are marked in the diagram. A - First crack in the experiment. B - Right before failure in the experiment. C - First crack in the FE-analysis. D - Final load step in the FE-analysis. Note the different scale in the diagram compared to the other beams.

5.2.3 Beam 3

In both the experiment and the FE-analysis, the cracks localised in a few larger cracks, these grow in size until tensile failure of the reinforcement occurred, see Figure 5.7. A difference between the two is that the beam in the experiment had some crack propagation into additional cracks, resulting in a slightly more ductile behaviour in comparison with the beam in the FE-analysis which had a brittle behaviour.

In the FE-analysis, the maximum compressive stress in the concrete was 7.0 [MPa] which is lower than the compressive strength of the concrete. However, the maximum stress in the reinforcement reached its capacity, which led to tensile failure of the reinforcement in Beam 3 at point D in the diagram in Figure 5.7.

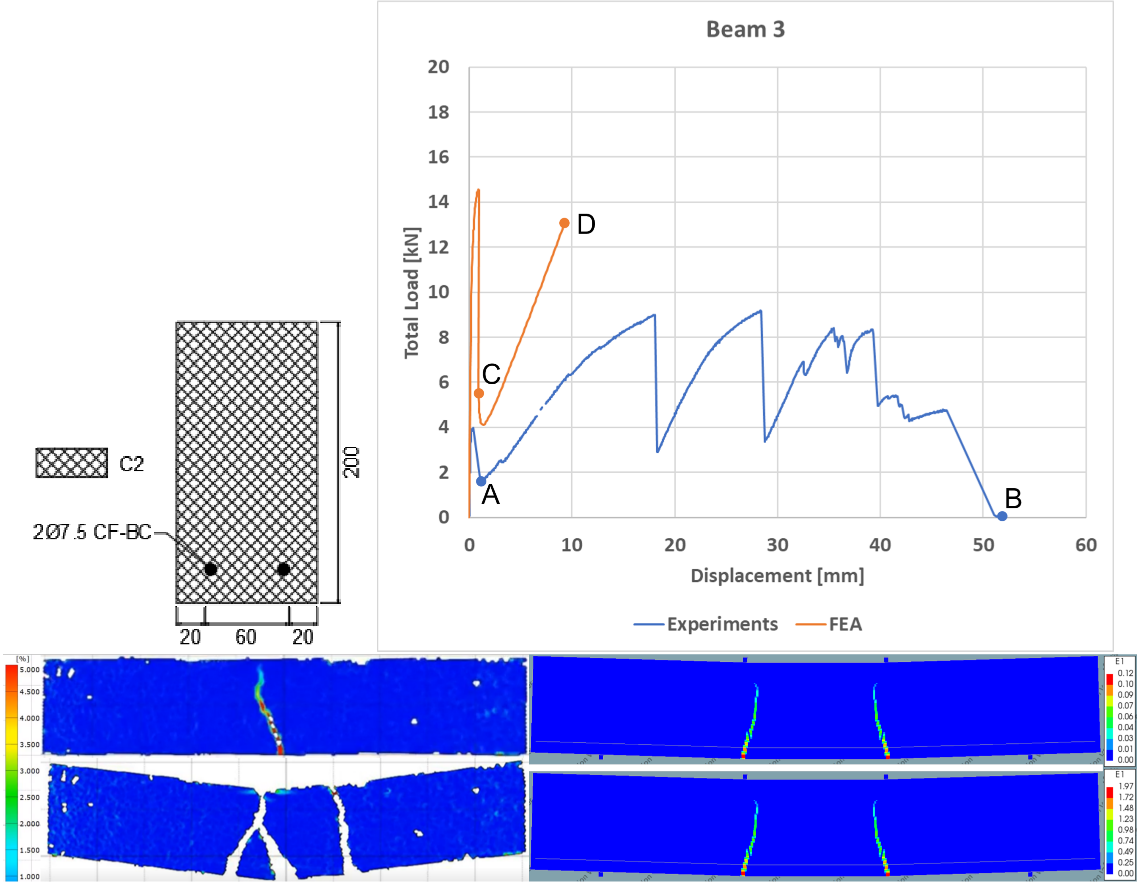

Figure 5.7: The cross-section for Beam 3 is presented together with the results of the experiment and the FE-analysis. The crack patterns at different stages are marked in the diagram. A - First crack in the experiment. B - Right before failure in the experiment. C - First crack in the FE-analysis. D - Final load step in the FE-analysis.

5.2.4 Beam 4

In the experiment, the cracks spread evenly between the supports which resembles the behaviour seen for the steel reinforced beam, Beam 1. The failure of the beam came from pull-out of the reinforcement close to the left support, see Figure 5.8. This was due to the low bond strength between the SB-reinforcement and the concrete. When the reinforcement started to slip, the shear crack increased rapidly in size and the load capacity decreased. Since Beam 4 had SB-reinforcement and no tensile failure occurred in the pull-out experiments, no FE-analysis was performed for this beam.

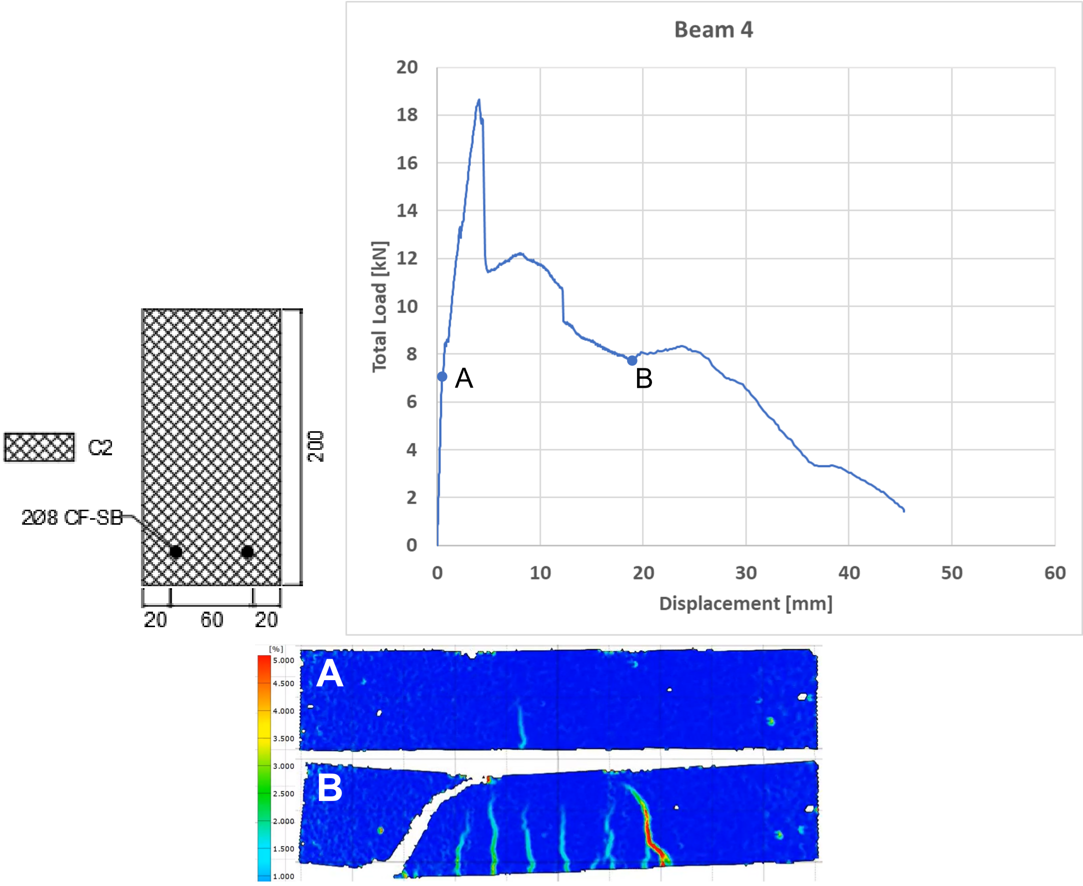

Figure 5.8: The cross-section for Beam 4 is presented together with the results of the experiment. The crack patterns at different stages are marked in the diagram. A - First crack in the experiment. B - Right before the large pull-out of the reinforcement occur.

5.2.5 Beam 5

In the experiment, the crack pattern was localised to a single crack located near one of the loading points. In the FE-analysis, however, two cracks are observed closer to the center of the beam, as illustrated in Figure 5.9. Furthermore, in the experiment, the deformation in the initial crack increased, instead of, propagation into additional cracks. As a consequence, the deformation proceeds without any substantial increase in the applied load until the reinforcement breaks. The absence of additional cracks signifies a brittle behavior. Additionally, cracks along the reinforcement were also observed in the experiment, both at the top and bottom sections.

In the FE-analysis, the maximum compressive stress in the concrete was 22.8 [MPa] which is lower than the compressive strength of the concrete. However, the maximum stress in the reinforcement reached its capacity, which lead to tensile failure of the reinforcement in Beam 5 at point D in the diagram in Figure 5.9.

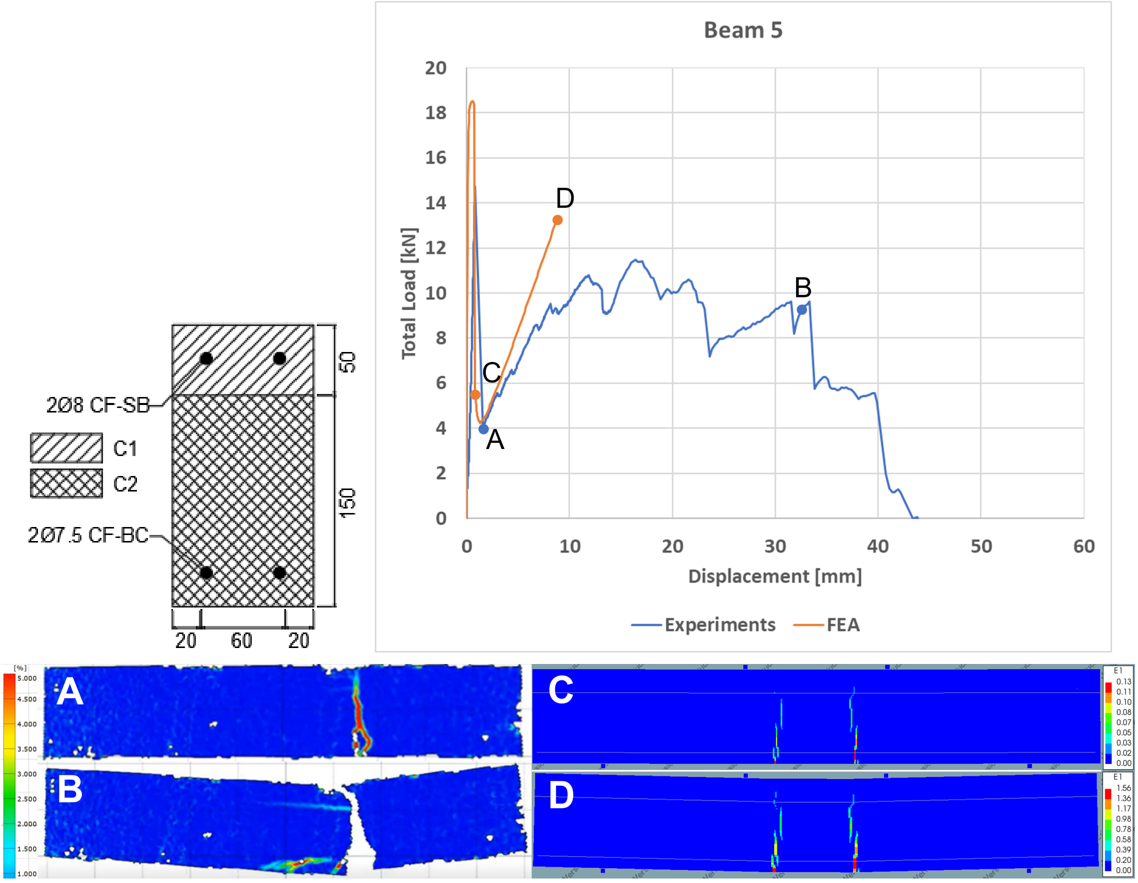

Figure 5.9: The cross-section for Beam 5 is presented together with the results of the experiment and the FE-analysis. The crack patterns at different stages are marked in the diagram. A - First crack in the experiment. B - Right before failure in the experiment. C - First crack in the FE-analysis. D - Final load step in the FE-analysis.

5.2.6 Beam 6

For Beam 6, two experiment beams were tested, called Beam 6 and 6´. Both beams in the experiments displayed a ductile behaviour, with multiple cracks propagating, see Figure 5.10. In the graph it is distinguishable where the cracks appear, it is shown by the larger changes of the applied load. In the FE-analysis the cracks localised into two cracks only.

In the FE-analysis, the maximum compressive stress in the concrete was 24.7 [MPa] which is lower than the compressive strength of the concrete. However, the maximum stress in the reinforcement reached its capacity, which led to tensile failure of the reinforcement in Beam 6 at point F in the diagram in Figure 5.10.

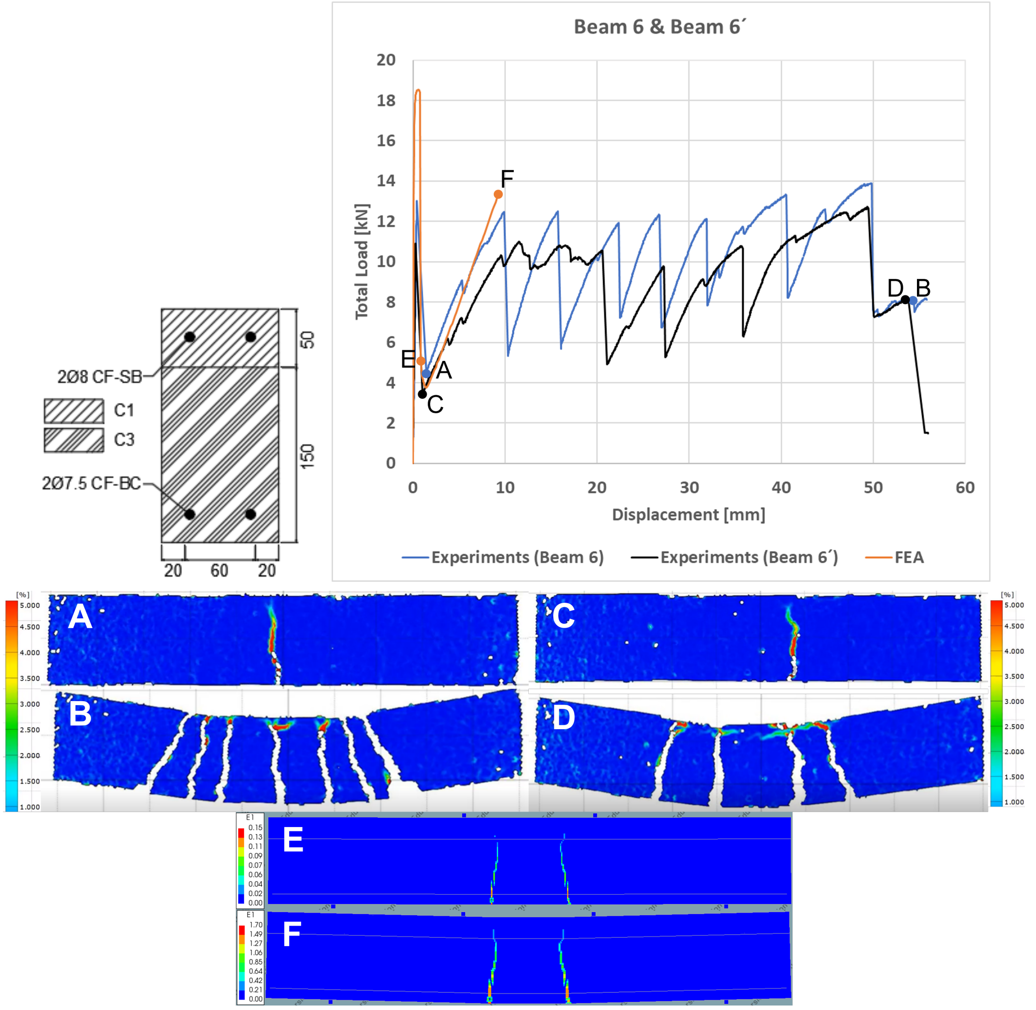

Figure 5.10: The cross-section for Beam 6 is presented together with the results of the experiment and the FE-analysis. The crack patterns at different stages are marked in the diagram. A - First crack in the experiment (Beam 6). B - Right before failure in the experiment (Beam 6). C - First crack in the experiment (Beam 6´). D - Right before failure in the experiment (Beam 6´). E - First crack in the FE-analysis. F - Final load step in the FE-analysis.

5.2.7 Beam 7

In the experiment, one central crack only appeared, while in the FE-analisys there were two cracks closer to the loading points, see Figure 5.11. In the experiment large lateral cracks occurred at the bottom along the reinforcement. This resulted in loss of contact between the reinforcement and the concrete in the cracked section. For this beam, the experiment was stopped before tensile failure of the reinforcement occurred.

In the FE-analysis, the maximum compressive stress in the concrete was 15.6 [MPa] which is lower than the compressive strength of the concrete. However, the maximum stress in the reinforcement reached its capacity, which led to tensile failure of the reinforcement in Beam 7 at point D in the diagram in Figure 5.11.

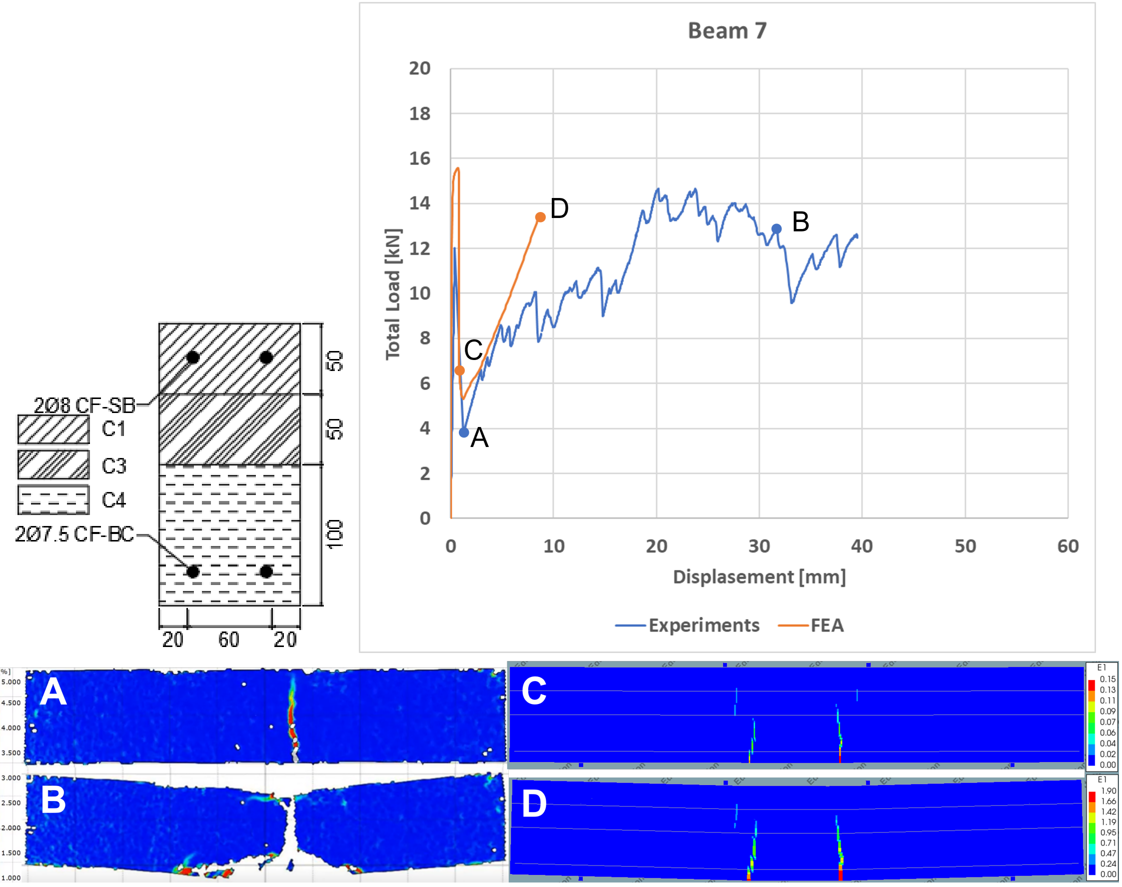

Figure 5.11: The cross-section for Beam 7 is presented together with the results of the experiment and the FE-analysis. The crack patterns at different stages are marked in the diagram. A - First crack in the experiment. B - Right before failure in the experiment. C - First crack in the FE-analysis. D - Final load step in the FE-analysis.

5.2.8 Beam 8

In the experiment, only one crack at mid span appeared, see Figure 5.12. Large lateral cracking occurred at the bottom along the reinforcement, thus resulting in loss of contact between the reinforcement and the concrete in the cracked section. The maximum capacity of the beam was slightly larger compared to the other beams reinforced with BC-reinforcement, but this slight increase in capacity does not correlate with the increase of reinforcement amount. The reinforcement configuration with bundled cords seemed to result in uneven stress distribution between the cords: some of the cords were subjected to tensile failure and some remained intact during the testing of the beam. Since no pull-out experiment was performed for three braided cords bundled together, no FE-analysis was conducted for Beam 8.

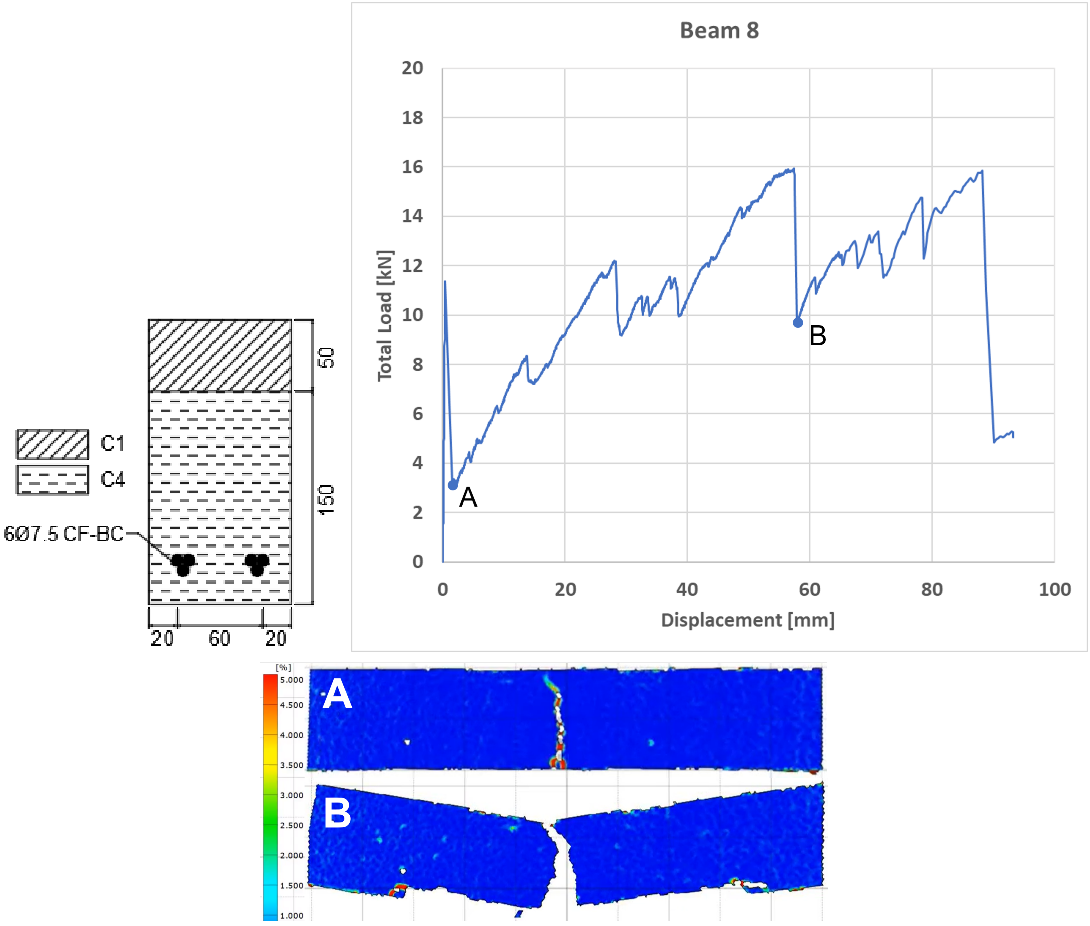

Figure 5.12: The cross-section for Beam 8 is presented together with the results of the experiment. The crack patterns at different stages are marked in the diagram. A - First crack in the experiment. B - Just prior to the significant deformations in the experiment. Note the different scale in the diagram compared to the other beams.

5.3 General observations and comparisons

The analysis demonstrated that the utilisation of the carbon fibres and the low bond strength between the BC-reinforcement and the LWC were causes of concern. Large cracks were created even for quite low loads and this resulted in very low capacity after the first cracking of the concrete. In fact, the BC-reinforced beams were barely, or not at all, able to carry higher loads after first cracking occurred. This is a problem for the composite, as the composite is weaker after cracking than it was before. In contrast, the steel reinforced beams, where the composite was able to carry much higher loads when the reinforcement was activated. Only in one carbon-reinforced beam could the load be increased after the first crack: for Beam 4 with SB-reinforcement, which also displayed a similar crack propagation as the reference beam, Beam 1. However, the low bond properties resulted in pull-out failure before the reinforcement could be used to its full potential. It is interesting to compare the utilisation of the strength of the carbon reinforcement in this four-point bending test with the corresponding one in the pull-out test with 300mm of anchorage length, SB-300. Which had a utilisation ratio of the tensile strength, U_{σ_s}, of 0.97[%], see Table 5.1. In the four-point bending test the pull-out happened around 260mm from the end of the beam at the shear crack and the utilisation ratio of the tensile strength in the reinforcement, U_{σ_s}, was 4.5[%], see Table 5.3. Which means that the utilisation of the reinforcement was substantially higher in the four-point bending test than in the pull-out test. A possible reason could be that the reaction force from the support is increasing the frictional force between the concrete and the reinforcement. Beam 4 also have the highest utilisation of the reinforcement strength of all the beams with carbon reinforcement and was the only one with SB-reinforcement, see Table 5.3. Thus, the braiding seemed to decrease the capacity of the carbon. Yet, for the straight bundles, anchorage capacity is indeed an issue.

6

Applications

The experiments have underlined the low utilisation rate and brittle behaviour of the carbon reinforcement. The low bond strength between the materials leads to long required anchorage length. Still, it is difficult for the reinforcement to transfer the loads in an efficient way. In addition, when the cracking starts, the crack grows rapidly in size. As a result, the material is not suitable for applications where ductile behaviour and a high load capacity after cracking are required. One benefit of using CFR is that it does not corrode. This makes the material effective in keeping its strength properties for a long time even when used in harsh environments. Suggested applications for this material are therefore focused on concrete structures subjected to low tensile forces and in chloride environment. In the following sections, a few suggested applications are presented. Most of the suggested applications are mainly described and discussed, while for one of them (stocky columns), a FE-analysis was conducted.

6.1 Stocky columns

Stocky columns constructed in a marine environment are an interesting application. In this study, FE-models were created and analysed for such stocky columns. The models created had a height of 1[m], and a circular cross section with a diameter of 0.4[m]. The concrete used in the models was C2, which corresponds to the same concrete utilised in previous FE analyses, see Table 4.4. The reinforcements used in the models was shaped like a coil with an inner diameter of 0.34[m]. The coil reached from the bottom to the top of the columns in 20 evenly spaced laps. The configuration of the reinforcement coil was chosen to have a spacing between the laps of around 4[cm]. Two different reinforcement types were used in the two separate analyses. One column had the same steel reinforcement as the one used in the reference beam, Beam 1, see Table 4.5. In the other column, the same BC-reinforcement as in the previous analysis was used, see Table 4.2. To make relevant comparisons, the reinforcement configuration was identical in the models, except the reinforcement area which is 8[mm] in the steel coil and 7.5[mm] in the BC coil. The bottom of each column was rigidly fixed, preventing any movement or rotation in any direction. A distributed load was applied on the top of the column, and increased stepwise until failure took place, see Figure 6.1. The intention was to see how large load it takes for the columns to break, after the lateral confinement is created.

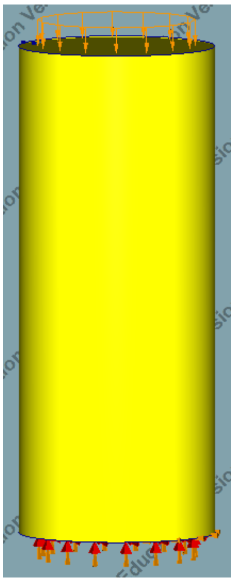

Figure 6.1: Model of a stocky column, with distributed load on top and boundary conditions on the bottom.

A convergence study was conducted on the column with BC-reinforcement, with element sizes of 0.02, 0.04, 0.08 and 0.16[m], see Figure 6.2. The convergence study resulted in an element size of 0.04[m].

Coiling the reinforcement around the outer edge of the columns, are creating a lateral confinement which increase the load-bearing capacity. The aim of this analysis was to compare how much the load-bearing capacity was increased when applying the different reinforcement types. Due to the stockiness of the columns, the second order effects can be disregarded in the models.

The total load that was applied at failure for the reference column was 2680[kN] which correspond to the compressive strength of the concrete. The analyses showed a small increase in load capacity using BC-reinforcement of roughly 2[%] compared to the column without reinforcement. The capacity of the steel reinforced column was roughly 8[%] larger than the column without reinforcement; thus the increase in capacity was larger for the steel-reinforced than the carbon-reinforced column. It is worth to note that both types of reinforcement have substantial tensile capacity left. The tensile stress is a bit higher in the BC-reinforcement than in the steel reinforcement, but due to the low utilization of the reinforcement area of the BC-reinforcement, the force in the steel reinforcement is much larger than for the BC-reinforcement. In Table 6.1 the capacity increase and reinforcement stress and forces are displayed. The failure mode was crushing of the concrete in all analyses. The differences in load capacity for the different reinforcement types are displayed in Figure 6.2. The stress distribution within the reinforcement can be seen in Figure 6.3.

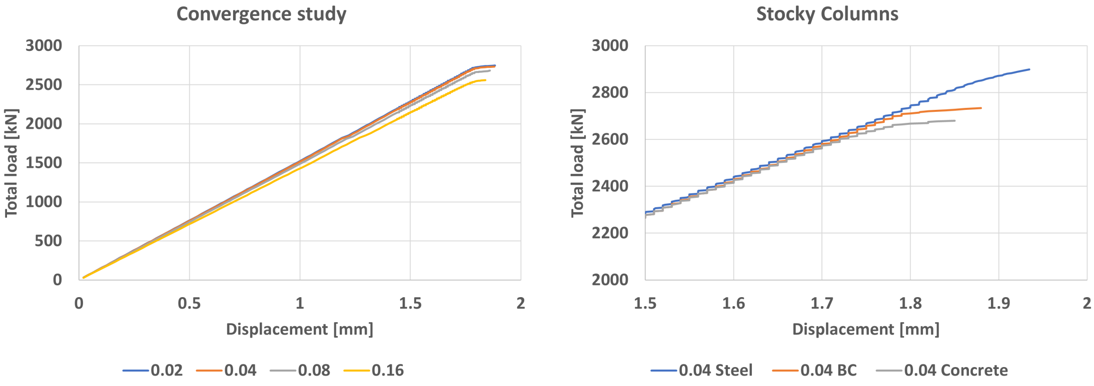

Figure 6.2: Left diagram show the convergence study. The right diagram are showing the differences in load-carrying capacity between the various columns. Note the different scales.

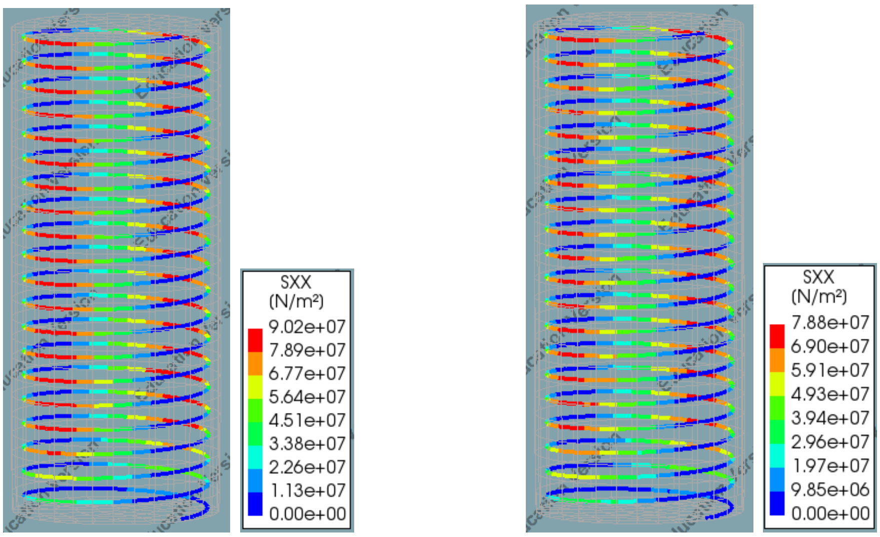

Figure 6.3: Pictures of the reinforcement stresses and tables over the highest stress in the reinforcement. In the left picture the BC-reinforcement is shown and in the right the steel reinforcement is shown.

Table 6.1: Table with maximum load and capacity increase for each column, and maximum reinforcement stress and force for the columns with steel and BC-reinforcement

Type	Concrete	Steel	BC
Maximum load [kN]	2680	2899	2734
Capacity increase [%]	Reference	+8	+2
Maximum reinforcement stress [MPa]	-	78.8	90.2
Maximum reinforcement force [kN]	-	3.961	0.133

6.2 Floating pontoons

Floating pontoons is an example of another application subjected to low tensile stresses and chloride environment. The lightness of the concrete is also beneficial for the pontoons as it creates less down force than regular heavy concrete. The loads on the surface of the pontoons is mostly compression due to water pressure. The loads are also relatively low, which excludes the risk of cracking of the concrete. Potential challenges include the load induced by the freezing of the surrounding water or the risk of an impact load. Hence, if the pontoons were to be used in a cold climate or be affected by impact, e.g. collision by boats, these would need strengthening.

6.3 Culvert

Concrete culverts used for transferring water or sewage is also an appropriate application for the material. In this application a round shape is preferred, as the round shape distributes the load in compression.

6.4 Edge beams

Edge beams in bridges are exposed to a harsh climate with road salts and moisture, which cause the concrete to disintegrate, and the reinforcement to degrade if steel reinforcement is used. The primary function of the edge beams is to support the pavement and the railing in bridge systems, so there is no need for high load capacity of the elements. However, the risk for cracking due to restraint forces as well as the risk for impact loads, makes it questionable if the material is suitable for this application. To be able to reduce the crack widths coming from the restraint cracking, a better bond strength is needed between the concrete and the BC-reinforcement, and to be able to secure the impact loads better ductility is needed.

6.5 Discussion

Possible applications of the material was considered: stocky columns, floating pontoons, culverts and edge beams. It was difficult to come up with structural applications for the composite in question. For most applications, it is crucial for concrete structures to have a large load-carrying capacity after cracking, and a ductile behaviour is also most often highly desirable. Due to the brittleness of the material, the only applications that were considered relevant were when concrete was not exposed to cracking due to tensile stresses. One application that may be of interest is the stocky columns where the reinforcement is able to create a lateral confinement, thus, creating a composite the has a slightly better load carrying capacity, but still not as good as with steel reinforcement.

7

Conclusions

The results obtained from the pull-out experiments revealed a significant weakness in the bond strength between the carbon reinforcement and the concrete. This weakness creates a need for the use of longer anchorage lengths. However, simply increasing the anchorage length does not resolve the issue, as interfilament slip within the reinforcement leads to a low utilisation of its strength. In the four-point bending tests, the beams reinforced with CFR exhibited the occurrence of large cracks, and failure took place at significantly lower loads compared to the reference beam. One notable distinction between the SB-reinforcement and the BC-reinforcement lies in the stronger bond between the BC-reinforcement and the concrete.

During the beam tests, the SB-reinforced beam demonstrated a higher load-carrying capacity than all BC-reinforced beams. The FE-model developed for simulating the pull-out experiments yielded comparable results to the actual experiments. The bond-slip model implemented for the BC-reinforcement also proved effective when applied in the FE-analyses of the beams loaded in four-point bending, producing results in close agreement with the experimental data. One difference though, was that, the FE-analyses did not exhibit the propagation of additional cracks, which was seen in some of the experiments.

The material model was employed for a study of stocky columns with BC-reinforcement, which was compared with models of steel-reinforced and unreinforced columns. The load-carrying capacity of the reinforced column surpassed that of the unreinforced column, yet it was smaller than the load capacity observed in the steel-reinforced column. As a suggestion for future research, it would be valuable to investigate the composite's behavior under different carbon reinforcement impregnation methods. Improved impregnation is likely to enhance bond properties and enable a more efficient utilisation of the reinforcement, leading to an overall improvement in composite performance. This, in turn, could position LWAC with CFR as a viable option for structural elements, particularly in chloride-rich environments where the composite could offer significant advantages.

In conclusion, this thesis aims to provide valuable insights for future research endeavors in this field. It is hoped that the findings presented contribute to the advancement of knowledge and pave the way for the integration of LWAC with CFR in the construction of structural components.

References

Abd, S. M., Mhaimeed, I. S., Tayeh, B. A., Najm, H. M., & Qaidi, S. (2023, 7). Investigation of the use of textile carbon yarns as sustainable shear reinforcement in concrete beams. *Case Studies in Construction Materials*, *18*. doi: 10.1016/j.cscm.2022.e01765

Bilek, V., Bonczková, S., Hurta, J., Pytlík, D., & Mrovec, M. (2017). Bond Strength between Reinforcing Steel and Different Types of Concrete. In *Procedia engineering* (Vol. 190, pp. 243–247). Elsevier Ltd. doi: 10.1016/j.proeng.2017.05.333

Bogas, J. A., Carriço, A., & Pontes, J. (2019, 11). Influence of cracking on the capillary absorption and carbonation of structural lightweight aggregate concrete. *Cement and Concrete Composites*, *104*. doi: 10.1016/j.cemconcomp.2019.103382

Bogas, J. A., & Real, S. (2019, 10). *A review on the carbonation and chloride penetration resistance of structural lightweight aggregate concrete* (Vol. 12) (No. 20). MDPI AG. doi: 10.3390/ma12203456

Bremner, T. W. (2008). Lightweight concrete. In S. Mindess (Ed.), *Developments in the formulation and reinforcement of concrete* (pp. 167–186). Brunswick: Woodhead Publishing. doi: https://doi.org/10.1533/9781845694685.167

Burström, P. G., & Nilvér, K. (2018). *Byggnadsmaterial: tillverkning, egenskaper och användning* (3rd ed.). Lund: Studentlitteratur AB.

Byard, B. E., & Schindler, A. K. (2010). *CRACKING TENDENCY OF LIGHTWEIGHT CONCRETE* (Tech. Rep.). Retrieved from `https://www.escsi.org/wp-content/uploads/2017/10/ESCSI-Final-Report-Auburn-University.pdf`

Carolin, A. (2003). *Carbon Fibre Reinforced Polymers for Stengthening of Structural Elements* (Unpublished doctoral dissertation). Structural Engineering, Luleå.

Duan, S., Liu, F., Pettersson, T., Creighton, C., & Asp, L. E. (2019, 3). Determination of transverse and shear moduli of single carbon fibres. *Carbon*, *158*, 772–782. doi: 10.1016/j.carbon.2019.11.054

European committee for standardization. (2004). *Eurocode 2: Design of concrete structures-Part 1-1: General rules and rules for buildings* (Tech. Rep.). Retrieved from `https://www-sis-se.eu1.proxy.openathens.net/produkter/byggnadsmaterial-och-byggnader/byggnadsindustrin/tekniska-aspekter/ssen19921120052/`

Firty, A. (2012). The unhistorical and the historical are necessary in equal measure for the health of an individual, of a people and of a culture. In A. Forty (Ed.), *Concrete and culture: A material history* (1st ed., pp. 79–100). London. Retrieved from `http://ebookcentral.proquest.com/lib/chalmers/detail.action?docID=1127624.`

Friese, D., Scheurer, M., Hahn, L., Gries, T., & Cherif, C. (2022, 11). *Textile reinforcement structures for concrete construction applications—a review* (Vol. 56) (No. 26). SAGE Publications Ltd. doi: 10.1177/00219983221127181

Gore, A. (2007). *An Inconvenient Truth: The Crisis of Global Warming.* New York: Viking/Rodale.

Haque, M. N., Al-Khaiat, H., & Kayali, O. (2004, 5). Strength and durability of lightweight concrete. *Cement and Concrete Composites*, *26*(4), 307–314. doi: 10.1016/S0958-9465(02)00141-5

Hegger, J., & Voss, S. (2008, 7). Investigations on the bearing behaviour and application potential of textile reinforced concrete. *Engineering Structures*, *30*(7), 2050–2056. doi: 10.1016/j.engstruct.2008.01.006

IEA, & GlobalABC. (2019). *2019 Global Status Report for Buildings and Construction.* International Energy Agency.

IPCC. (1988, 11). *First Session of the IPCC (IPCC-1)* (Tech. Rep.). Geneva: World Meterological Organization.

Junaid, M. F., Rehman, Z. u., Kuruc, M., Medveď, I., Bačinskas, D., Čurpek, J., . . . Ansari, W. S. (2022, 2). Lightweight concrete from a perspective of sustainable reuse of waste byproducts. *Construction and Building Materials*, *319*. doi: 10.1016/j.conbuildmat.2021.126061

Kanavaris, F., Gibbons, O., Walport, E., Shearer, E., Abbas, A., Orr, J., & Marsh, B. (2020). *Reducing the carbon footprint of lightweight aggregate concrete* (Tech. Rep.). Kentucky: International Conference on Low Carbon Cement and Concrete. Retrieved from `https://www.researchgate.net/publication/344501000`

Lo, T. Y., Tang, W. C., & Nadeem, A. (2008, 8). Comparison of carbonation of lightweight concrete with normal weight concrete at similar strength levels. *Construction and Building Materials*, *22*(8), 1648–1655. doi: 10.1016/j.conbuildmat.2007.06.006

Mechtcherine, V., Michel, A., Liebscher, M., & Schmeier, T. (2020, 6). Extrusion-based additive manufacturing with carbon reinforced concrete: Concept and feasibility study. *Materials*, *13*(11). doi: 10.3390/ma13112568

Mirdarsoltany, M., Abed, F., Homayoonmehr, R., & Alavi Nezhad Khalil Abad, S. V. (2022, 7). *A Comprehensive Review of the Effects of Different Simulated Environmental Conditions and Hybridization Processes on the Mechanical Behavior of Different FRP Bars* (Vol. 14) (No. 14). MDPI. doi: 10.3390/su14148834

Moussard, M., Garibaldi, P., & Curbach, M. (2018). The invention of reinforced concrete (1848-1906). In *fib symposium* (pp. 2785–2794). fib. The International Federation for Structural Concrete. doi: 10.1007/978-3-319-59471-2{_}316

Schneider, K., Michel, A., Liebscher, M., Terreri, L., Hempel, S., & Mechtcherine, V. (2019, 3). Mineral-impregnated carbon fibre reinforcement for high temperature resistance of thin-walled concrete structures. *Cement and Concrete Composites*, *97*, 68–77. doi: 10.1016/j.cemconcomp.2018.12.006

Sciegaj, A., Larsson, F., & Lundgren, K. (2022, 11). Experiments and calibration of a bond-slip relation and efficiency factors for textile reinforcement in concrete. *Cement and Concrete Composites*, *134*. doi: 10.1016/j.cemconcomp.2022.104756

Scope, C., Guenther, E., Schütz, J., Mielecke, T., Mündecke, E., Schultze, K., & Saling, P. (2020, 12). Aiming for life cycle sustainability assessment of cement-based composites: A trend study for wall systems of carbon concrete: Dresden Nexus Conference 2020—Session 4—Circular economy for building with secondary construction materials to minimise resource use and land use. *Civil Engineering Design*, *2*(5-6), 143–158. doi: 10.1002/cend.202000024

Stern, N. (2007). *Climate Change: The Stern Review.* Cambridge: Cambridge University Press.

Stoiber, N., Hammerl, M., & Kromoser, B. (2021, 1). Cradle-to-gate life cycle assessment of CFRP reinforcement for concrete structures: Calculation basis and exemplary application. *Journal of Cleaner Production*, *280*. doi: 10.1016/j.jclepro.2020.124300

Tang, L. (2022). *Carbon Fibre Textile Reinforced Lightweight Concrete with Green Binder and Recycled Aggregates* (Tech. Rep.).

Zhu, M., Zhu, J. H., Ueda, T., Matsumoto, K., & Su, M. (2021, 4). Bond behavior of carbon fabric reinforced cementitious matrix (FRCM) composites considering matrix impregnation. *Composite Structures*, *262*. doi: 10.1016/j.compstruct.2020.113350

Zivkovic, J., Lukovic, M., Overli, J. A., & Hordijk, D. (2018, 10). Brittleness of high-strength lightweight aggregate concrete. In *Synercrete'18 international conference on interdisciplinary approaches for cement-based materials and structural concret8.* Funchal: TU Delft. Retrieved from `https://www.researchgate.net/publication/331231809`

A

Appendix 1

A.1 Pull-out test

In Table A.1, the embedded lengths, l, and tensile strengths of the reinforcement, f_t, presented together with the maximum force, F_{max}, obtained from the tests. For the BC-reinforcement, the lowest value from the manufacturer was chosen for f_t.

Table A.1: Input data from the test set-ups (embedded length, l, and tensile strength, f_t) and the maximum force, F_{max}, obtained in the tests.

Specimen	SB-75	SB-150	SB-300	BC-75	BC-50	BC-65
l [mm]	75	150	300	75	50	65
f_t [MPa]	4000	4000	4000	3530	3530	3530
F_{max} [kN]	1.194	1.590	1.943	5.216	3.663	3.620

The diameter of the reinforcements, $\varnothing$, was $0.008m$ for the specimens with SB-reinforcement and $0.0075m$ for the specimens with BC-reinforcement. The area, A_s for each type in Eq. A.1-A.2.

$$A_{s,SB} = \frac{\pi \times \varnothing^2}{4} = \frac{\pi \times 0.008^2}{4} = 5.02655 \times 10^{-5} m^2 \tag{A.1}$$

$$A_{s,BC} = \frac{\pi \times \varnothing^2}{4} = \frac{\pi \times 0.0075^2}{4} = 4.41786 \times 10^{-5} m^2 \tag{A.2}$$

From the values in Table A.1 and the area of the reinforcement was the tensile stress in the reinforcement, $\sigma_{s,max}$, the utilisation ratio of the tensile stress, U_{σ_s}, and the shear stress between the concrete and the reinforcement calculated, see Eq. A.3-A.5 and Table A.2.

$$\sigma_{s,max} = \frac{F_{max}}{A_s} \tag{A.3}$$

$$U_{\sigma_s} = \frac{\sigma_{s,max}}{f_t} \tag{A.4}$$

$$\tau_b = \frac{F_{max}}{\pi \times \varnothing \times l} \tag{A.5}$$

Table A.2: Calculated values of maximum stresses, the utilisation ratio of the reinforcement strength and the maximum mean shear stresses between the concrete and the reinforcement.

Specimen	SB-75	SB-150	SB-300	BC-75	BC-50	BC-65
$\sigma_{s,max}$ [MPa]	23.744	31.640	38.656	118.077	82.910	81.950
U_{σ_s} [%]	0.59	0.79	0.97	3.34	2.35	2.32
τ_b [MPa]	0.633	0.422	0.258	2.952	3.109	2.364

A.1.1 Inter-filament slip

Inter-filament slip can only be analysed from the test where the reinforcement are exposed to tension failure. Tension failure happened for the BC-reinforcement with an embedded length of 75mm, BC-75. In the analyse, the inner filaments in the reinforcement was assumed to not contribute to the load carrying and the stresses in the inner filaments are therefore set to zero. The utilised area with full bond to the LWC was expected to have an even stress distribution between filaments and the maximum stress in the filaments was set to $f_t = 3530 MPa$, the lowest strength value given by the manufacturer.

The inter-filament slip leads to a lower utilisation of the area and the utilised area, $A_{s,utilised,BC-75}$, and the utilised ratio, U_{A_s}, was calculated with Eq. A.6 and A.7.

$$A_{s,utilised,BC-75} = \frac{F_{max,BC-75}}{f_{t,BC-75}} = 1.478 \times 10^{-6} m^2 \tag{A.6}$$

$$U_{A_s} = \frac{A_{s,utilised,BC-75}}{A_s} = 3.34\% \tag{A.7}$$

The diameter of the area that's not utilised was calculated with Eq. A.8-A.11 and the result is visualised in Figure A.1.

$$A_s = A_{s,utilised,BC-75} + \frac{\pi \times d^2_{notutilised,BC-75}}{4} \tag{A.8}$$

$$\Rightarrow \frac{\pi \times d^2_{notutilised,BC-75}}{4} = A_s - A_{s,utilised,BC-75} \tag{A.9}$$

$$\Rightarrow d_{notutilised,BC-75} = \sqrt{\frac{(A_s - A_{s,utilised,BC-75}) \times 4}{\pi}} = 0.00737 m = 7.37 mm \tag{A.10}$$

$$\frac{d_{notutilised,BC-75}}{\varnothing} = 98.31\% \tag{A.11}$$

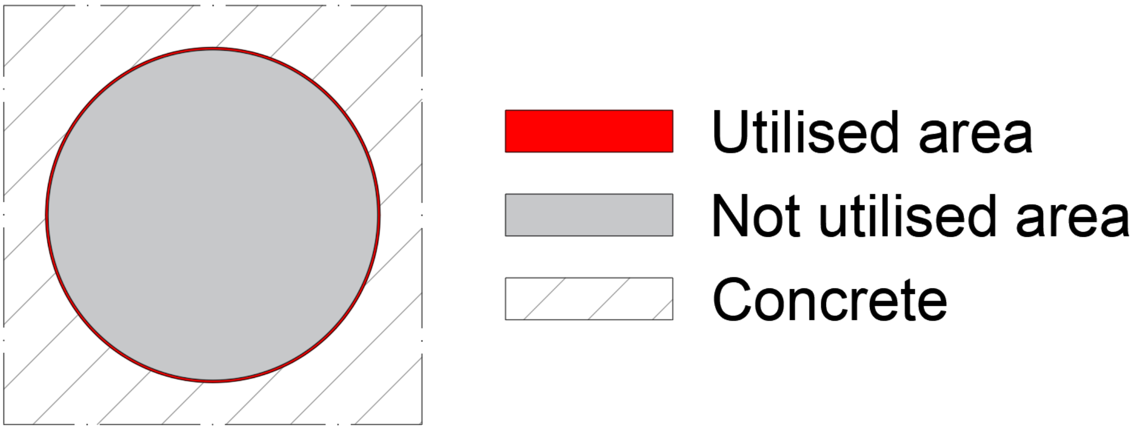

Figure A.1: Showing the ratios between utilised and not utilised area in the reinforcement cross-section.

A.2 Four-point bending test

A.2.1 Material data

The material data that was tested for each of the beams at the Structures Laboratory at Chalmers University of Technology, the compressive strength, f_{cm}, and the apparent density, ρ, was obtained from the tests. The values of each materials, modulus of elasticity, E_{cm}, and the concretes different tensile strengths, the 5-% fractile top value, $f_{ctk,0.95}$, and the bottom strength value, $f_{ctk,0.05}$, as well as the mean values of the tensile strength, f_{ctm}, was calculated using interpolation between the different categories in Table 3.1 in (European committee for standardization, 2004), see Table A.3.

Table A.3: Material properties for each of the concrete types. Values obtained by interpolation of values in Table 3.1 in EC2. Note that this not the final modulus of elasticity and tensile strengths of the types that are LWC.

Concrete type	C1	C2	C3	C4
$f_{cm}[MPa]$	49.8	21.6	19.2	17.5
$\rho[\frac{kg}{m^3}]$	2460	1450	1520	1260
$E_{cm}[GPa]$	35.36	27.80	26.60	25.75
$f_{ctk,0.05}[MPa]$	2.57	1.18	1.06	0.98
$f_{ctm}[MPa]$	3.61	1.75	1.55	1.25
$f_{ctk,0.95}[MPa]$	4.71	2.20	1.90	1.69

The factors η_E and η_1, see Eq. A.12-A.13 and Table A.4, are multiplied with the interpolated values in Table A.3 to obtain the final material properties for LWC, see Eq. A.14-A.17 and Table A.4. The equations taken from Table 11.3.1 in (European committee for standardization, 2004)

$$\eta_E = \left(\frac{\rho}{2200}\right)^2 \tag{A.12}$$

$$\eta_1 = 0.4 + 0.6 \times \frac{\rho}{2200} \tag{A.13}$$

$$E_{lcm} = E_{cm} \times \eta_E \tag{A.14}$$

$$f_{lctk,0.05} = f_{ctk,0.05} \times \eta_1 \tag{A.15}$$

$$f_{lctm} = f_{ctm} \times \eta_1 \tag{A.16}$$

$$f_{lctk,0.95} = f_{ctk,0.95} \times \eta_1 \tag{A.17}$$

Table A.4: Final material propeties for the LWC types.

Concrete type	C1	C2	C3	C4
$\eta_E[-]$	-	0.43	0.48	0.33
$\eta_1[-]$	-	0.8	0.81	0.74
$E_{lcm}[GPa]$	-	12.08	12.70	8.45
$f_{lctk,0.05}[MPa]$	-	0.94	0.86	0.73
$f_{lctm}[MPa]$	-	1.37	1.25	1.05
$f_{lctk,0.95}[MPa]$	-	1.75	1.55	1.25

A.2.2 Moment in four-point bending test

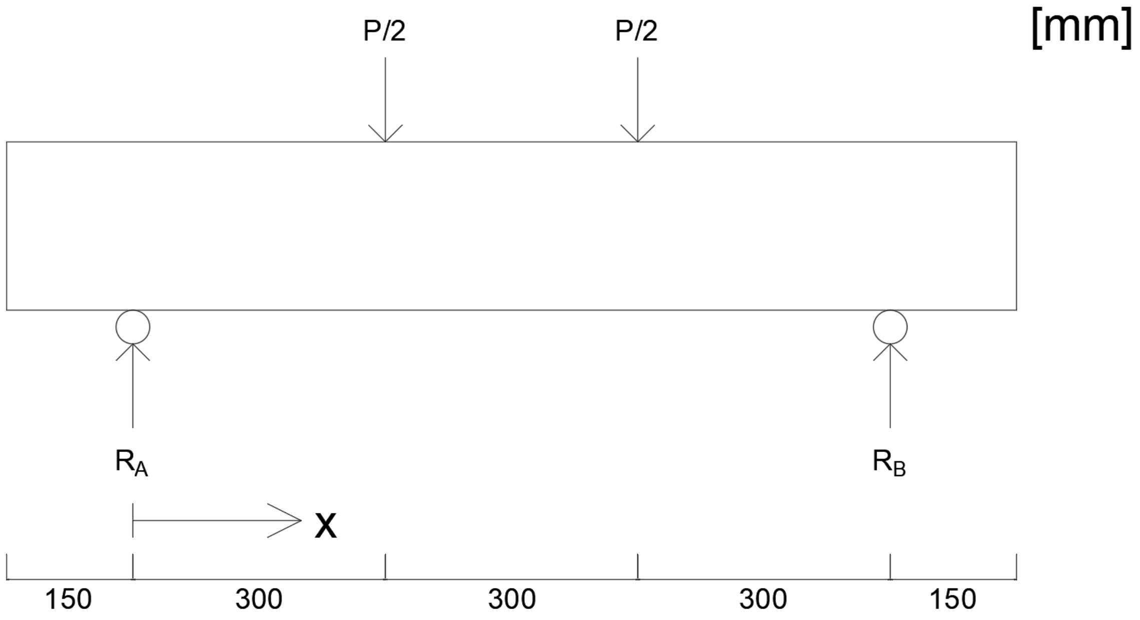

Figure A.2: Setup of the bending test with global measurements, loads and reaction forces.

Vertical equilibrium:

$$\uparrow\colon R_A + R_B - \frac{P}{2} - \frac{P}{2} = 0 \tag{A.18}$$

Due to symmetry:

$$R_A = R_B = \frac{P}{2} \tag{A.19}$$

Section at 0m $<$ x $\leq$ 0.3m:

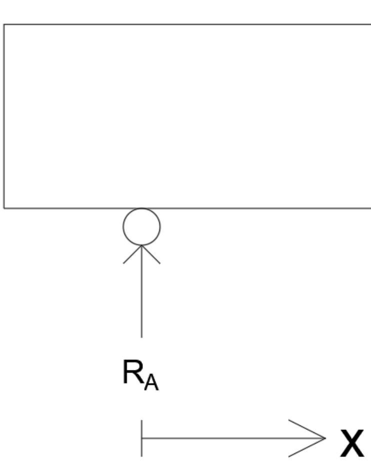

Figure A.3: Section at 0m $<$ x $\leq$ 0.3m.

Moment around x:

$$\curvearrowright\colon R_A \times x - M(x) = 0 \tag{A.20}$$

$$\Rightarrow M(x) = R_A \times x \tag{A.21}$$

$$\Rightarrow M(0.3) = \frac{P}{2} \times 0.3 \tag{A.22}$$

$$\Rightarrow M(0.3) = 0.15P \tag{A.23}$$

Section at 0.3m $\leq$ x $\leq$ $\frac{L}{2}$:

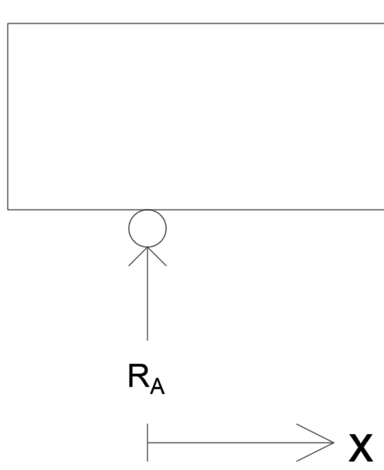

Figure A.4: Section at 0.3m $<$ x $\leq \frac{L}{2}$.

Moment around x:

$$\curvearrowright : R_A \times x - \frac{P}{2} \times (x - 0.3) - M(x) = 0 \tag{A.24}$$

$$\Rightarrow M(x) = R_A \times x - \frac{P}{2} \times (x - 0.3) \tag{A.25}$$

$$\Rightarrow M(0.45) = \frac{P}{2} \times 0.45 - \frac{P}{2} \times (0.45 - 0.3) = \frac{P}{2} \times (0.45 - 0.15) \tag{A.26}$$

$$\Rightarrow M(0.45) = 0.15P \tag{A.27}$$

Moment diagram between the supports:

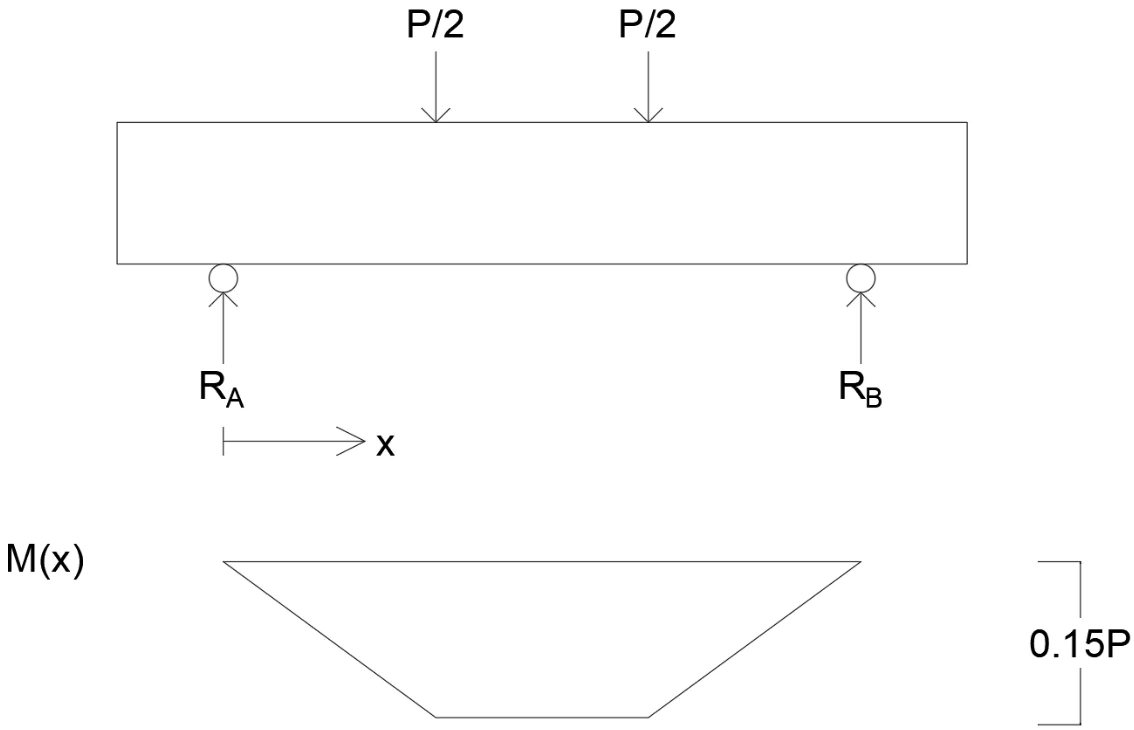

Figure A.5: Moment diagram in the beam between the supports. Maximum moment is 0.15P.

A.2.3 First crack

$$(A.26) \Rightarrow M_{cr} = 0.15 \times F_{cr} \tag{A.28}$$

$$I_I = \frac{b \times h^3}{12} = \frac{0.1 \times 0.2^3}{12} = 6.67 \times 10^{-5} m^4 \tag{A.29}$$

$$\sigma_{cr} = \frac{M_{cr}}{I_I} \times z \tag{A.30}$$

Table A.5: Showing the force in which the first crack appear in the concrete, as well as the cracking moment and the cracking stress for the first crack.

Beam	1	2	3	4	5	6	6’	7	8
F_{cr} [kN]	21.5	16.1	4.0	7.2	14.7	13.0	10.9	12.0	11.4
M_{cr} [kNm]	3.2	2.4	0.6	1.1	2.2	2.0	1.6	1.8	1.7
σ_{cr} [MPa]	4.8	3.6	0.9	1.6	3.3	2.9	2.5	2.7	2.6

A.2.4 Maximum stresses

The maximum stresses was calculated from the maximum moment, M_{max}, from the force-equilibrium in the cross-section, see Figure A.6.

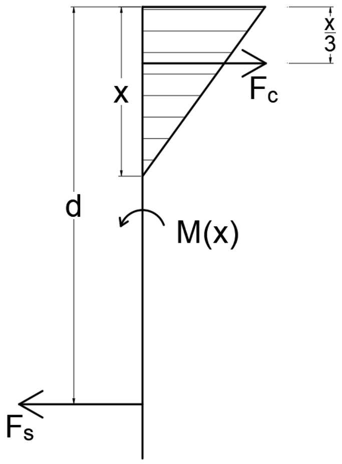

Figure A.6: Model over force-equilibrium in the cross-section in the beam after the first crack have appeared.

It can be seen in Figure 3.5 that Beam 5-8 has different layers of concrete. To adapt to this was the height of the compression zone, x, first assumed to be less than the height of the top layer, $x \leq \frac{1}{4}h$.

$$\alpha = \frac{E_s}{E_{cm}} \tag{A.31}$$

Table A.6: Young's modulus for the reinforcment and the concrete in the top of the beam, together with α and the number of reinforcement bars, n.

Beam	1	2	3	4	5	6	6'	7	8
E_s [GPa]	200	230	230	240	230	230	230	230	230
$E_{cm,top}$ [GPa]	35.36	35.36	12.08	12.08	35.36	35.36	35.36	35.36	35.36
α [-]	5.7	6.5	19.0	19.9	6.5	6.5	6.5	6.5	6.5
n [-]	2	2	2	2	2	2	2	2	6

$$A_s = \frac{\pi \times \varnothing^2}{4} \times n \tag{A.32}$$

$$(b \times x) \times \frac{x}{2} = \alpha \times A_s \times (d - x) \tag{A.33}$$

Table A.7: Reinforcement area, A_s, and neutral plane, x, for each of the beams tested in four-point bending

Beam	1	2	3	4	5	6	6'	7	8
A_s [10^{-4} m^2]	1.005	0.883	0.883	1.005	0.883	0.883	0.883	0.883	2.651
x [m]	0.039	0.040	0.062	0.066	0.040	0.040	0.040	0.040	0.062

For Beam 8: $x > \frac{h}{4}$ Not Ok! $\Rightarrow$ Assume $\frac{h}{4} \leq x \leq h$ (only for Beam 8):

$$E_{cm,bot,8} = 8.45GPa \tag{A.34}$$

$$\left(b \times \frac{h}{4}\right) \times E_{cm,top} \times \frac{\frac{h}{4}}{2} + \left(b \times \left(x - \frac{h}{4}\right)\right) \times E_{cm,bot} \times \left(\frac{h}{4} + \frac{x - \frac{h}{4}}{2}\right) = E_s \times A_s \times (d - x) \tag{A.35}$$

$$\Rightarrow x_8 = 0.076m \tag{A.36}$$

$$M_{max} = F_s \times \left(d - \frac{x}{3}\right) \tag{A.37}$$

$$\Rightarrow M_{max} = \sigma_{s,max} \times A_s \times \left(d - \frac{x}{3}\right) \tag{A.38}$$

$$\Rightarrow \sigma_{s,max} = \frac{M_{max}}{A_s \times \left(d - \frac{x}{3}\right)} \tag{A.39}$$

$$\frac{\sigma_{c,max}}{2} \times b \times x = \sigma_{s,max} \times A_s \tag{A.40}$$

$$\Rightarrow \sigma_{c,max} = \frac{2 \times \sigma_{s,max} \times A_s}{b \times x} \tag{A.41}$$

For Beam 1:

$$U_{\sigma_{s,max}} = \frac{\sigma_{s,max}}{f_{yk}} \tag{A.42}$$

For all beams except Beam 1:

$$U_{\sigma_{s,max}} = \frac{\sigma_{s,max}}{f_t} \tag{A.43}$$

$$U_{\sigma_{c,max}} = \frac{\sigma_{c,max}}{f_{ck,top}} \tag{A.44}$$

Table A.8: Results from the hand calculations for the beams tested in four-point bending.

Beam	1	2	3	4	5	6	6’	7	8
F_{max} [kN]	62.0	10.5	9.2	18.6	11.5	13.9	12.7	14.7	15.9
M_{max} [kNm]	9.3	1.6	1.4	2.8	1.7	2.1	1.9	2.2	2.4
$\sigma_{s,max}$ [MPa]	568.0	108.8	100.3	180.7	119.4	144.6	132.4	152.7	61.6
$\sigma_{c,max}$ [MPa]	29.0	4.9	2.9	5.5	5.3	6.5	5.9	6.8	4.3
$U_{\sigma_{s,max}}$ [%]	113.6	3.1	2.8	4.5	3.4	4.1	3.8	4.3	1.7
$U_{\sigma_{c,max}}$ [%]	58.2	9.7	13.2	25.4	10.7	13.0	11.9	13.7	8.6